Journal of Alzheimer's Disease 56 (2017) 1–23
DOI 10.3233/JAD-160761
IOS Press

Cholinergic Modification of Neurogenesis and Gliosis Improves the Memory of AβPPswe/PSEN1dE9 Alzheimer's Disease Model Mice Fed a High-Fat Diet

Takeshi Matsuda and Tatsuhiro Hisatsune*
Department of Integrated Biosciences, The University of Tokyo, Kashiwa, Japan

Handling Associate Editor: Shun Shimohama

Accepted 12 October 2016

Abstract. We previously reported that neuroinflammation contributes to the amnesia of AβPPswe/PSEN1dE9 Alzheimer's disease model mice fed a high-fat diet to induce type-2 diabetes (T2DM-AD mice), but the underlying mechanism for the memory decline remained unclear. Recent studies have suggested that cholinergic modulation is involved in neuroinflammatory cellular reactions including neurogenesis and gliosis, and in memory improvement. In this study, we administered a broad-spectrum cholinesterase inhibitor, rivastigmine (2 mg/kg/day, s.c.), into T2DM-AD mice for 6 weeks, and evaluated their memory performance, neurogenesis, and neuroinflammatory reactions. By two hippocampal-dependent memory tests, the Morris water maze and contextual fear conditioning, rivastigmine improved the memory deterioration of the T2DM-AD mice ($n=8$, $p<0.01$). The number of newborn neurons in the hippocampal dentate gyrus was 1138 ± 324 (Ave $\pm$ SEM) in wild-type littermates, 2573 ± 442 in T2DM-AD-Vehicle, and 2165 ± 300 in T2DM-AD-Rivastigmine mice, indicating that neurogenesis was accelerated in the two T2DM-AD groups ($n=5$, $p<0.05$). The dendritic maturation of new neurons in T2DM-AD-Vehicle mice was severely abrogated, and rivastigmine treatment reversed this retarded maturation. In addition, the hippocampus of T2DM-AD-Vehicle mice showed increased proinflammatory cytokines IL-1β and TNF-α and gliosis, and rivastigmine treatment blocked these inflammatory reactions. Rivastigmine did not change the insulin abnormality or amyloid pathology in these mice. Thus, cholinergic modulation by rivastigmine treatment led to enhanced neurogenesis and the suppression of gliosis, which together ameliorated the memory decline in T2DM-AD model mice.

Keywords: Acetylcholinesterase, Alzheimer's disease, gliosis, high-fat diet, inflammation, memory, neurogenesis, rivastigmine, type 2 diabetes mellitus

INTRODUCTION

Alzheimer's disease (AD) is the most prevalent form of dementia, and the number of patients with AD is increasing rapidly throughout the world [1, 2]. Although the pathogenic mechanism of AD is controversial, there is growing evidence that neuroinflammation underlies the cognitive decline in this disease [3–6]. Recent epidemiological studies revealed that type 2 diabetes mellitus (T2DM) is one of the strongest risk factors for AD [7–11]. Although the pathological relationship between AD and T2DM remains unclear, neuroinflammation is proposed to mediate this interactive pathology [12, 13].

Cholinesterase inhibitors are prescribed to inhibit the progression of dementia in the initial and middle stages of AD, although the working mechanism

*Correspondence to: Tatsuhiro Hisatsune, PhD, Department of Integrated Biosciences, The University of Tokyo, Kashiwanoha 5-1-5, Biosciences Bldg., Room 402, Kashiwa, Chiba 277-8562, Japan. Tel.: +81 4 7136 3632; Fax: +81 4 7136 3633; E-mail: hisatsune@k.u-tokyo.ac.jp.

is not fully understood [14–20]. The cholinesterase inhibitor rivastigmine is widely used to treat AD in clinical practice, and it is reported to effectively inhibit both acetylcholinesterase (AChE) and butyrylcholinesterase (BChE) [18–21]. Although BChE is conventionally considered to be a supportive enzyme for ACh degradation in the central nervous system, recent studies suggest that BChE is an important regulator of ACh levels, especially at extra-synaptic sites in the brain [22–26]. A decrease in the extra-synaptic ACh level downregulates anti-inflammatory signaling through the alpha7 nicotinic acetylcholine receptor (α7 nAChR) in microglia and provokes an elevation in proinflammatory cytokines [27, 28]. Rivastigmine indirectly activates α7 nAChR and inhibits various inflammatory reactions *in vitro* [29, 30]. These observations indicate that rivastigmine suppresses AD-associated neuroinflammation through cholinergic modulation.

Hippocampal neurogenesis is regulated by both cholinergic modulation and neuroinflammation. In the process of new-neuron maturation, neural progenitors and immature neurons receive cholinergic inputs from hippocampal circuits [31, 32], and their neuronal maturation is affected by surrounding inflammatory reactions [33]. A series of reports revealed the modulation of hippocampal neurogenesis in AD model mice. Most of these studies suggested that the rate of hippocampal neurogenesis is decreased in AD model mice [34–36], although some reports indicated that hippocampal neurogenesis is upregulated at some cell stages or mouse ages [37–41]. Nevertheless, the dysfunction of hippocampal neurogenesis is a potential candidate for the memory decline in AD model mice [42, 43]. While the cholinergic modulation of hippocampal neurogenesis is well understood [31, 32, 44–47], to the best of our knowledge, the effect of acetylcholinesterase inhibitors on the rate of hippocampal neurogenesis in AD model mice has been scarcely studied.

We previously reported that neuroinflammation, including the activation of microglia and astrocytes, is involved in the memory impairment of AβPPswe/PSEN1dE9 Alzheimer's disease model mice fed a high-fat diet to induce a type 2 diabetes mellitus (T2DM)-like pathology (T2DM-AD model mice) [48]. However, the underlying molecular pathogenesis and the microenvironmental cellular dynamics that support the memory system in the hippocampus remained to be elucidated. In this study, we investigated whether long-term treatment (6 weeks) with the AChE/BChE dual inhibitor rivastigmine could suppress neuroinflammatory reactions and prevent the AD-like memory deficits in this AD model mouse. We evaluated neuroinflammation using ELISAs for proinflammatory cytokines and immunostaining for neuroinflammatory markers such as astrocytes and microglial cells [48, 49]. We assessed the memory performance of the AD model mice using two hippocampal-dependent memory tasks, the Morris water maze and contextual fear conditioning [48, 50–52]. We also examined the level of adult hippocampal neurogenesis, both the number of new neurons and their dendritic maturation, as another sensitive indicator of neuroinflammation. Previous studies have shown that proinflammatory cytokines released by neuroinflammatory reactions downregulate the maturation of new neurons and inhibit the integration of new neurons into hippocampal circuits [33, 53–55]. A better understanding of the dynamics of hippocampal astrocytes, microglia, and neurons in the presence of neuroinflammation, and their alterations by cholinergic modulation, will provide valuable information for the development of new drugs and therapeutics targeting inflammation and intrinsic neural progenitors in AD.

MATERIALS AND METHODS

Animals

AβPPswe/PSEN1dE9 (AβPP/PS1) transgenic mice were used. The double-transgenic (Tg) mice were originally obtained from Jackson Laboratory (strain name B6C3-Tg (AβPPswe, PSEN1dE9) 85Dbo/J; stock number 004462), and were bred and raised in our laboratory for experiments. These B6C3-based Tg mice harbor two AD-related genes, one encoding a chimeric mouse/human amyloid-β protein precursor containing the K595N/M596L Swedish mutation (AβPPswe) and the other a mutant human presenilin 1 carrying a deletion of exon 9 (PSEN1dE9). The transgenes are controlled separately by mouse prion protein promoter elements, and are expressed predominantly in neurons in the central nervous system [56, 57]. The AβPP/PS1 Tg mice were maintained as double hemizygotes by interbreeding with wild-type (Wt) mice (B6C3F1/J background strain) purchased from Jackson Laboratory. In this study, we used male and female hemizygous Tg mice and their Wt littermates. Males and females were included approximately equally in each experimental group. The mice were genotyped from tail tissue as previously described [48]. Up

to three littermates were kept in one plastic cage. The cages were kept at a temperature of 23–25°C with a 12-h light-dark cycle. All animal procedures and experiments in this study were approved by our institution's ethics committee and were conducted according to the guidelines for animal experimentation required by the University of Tokyo.

Diet, food consumption, and weight

To create the T2DM-AD model mice, 4-month-old male and female AβPP/PS1 Tg mice were fed a high-fat diet (HFD) (HFD-32, CLEA Japan; its composition is shown in Supplementary Table 1) for 8 weeks from 4 months of age, which induces early-onset memory decline in the Tg mice at 6 months, as reported previously [48]. In agreement with our previous research [48], several studies have shown that AβPP/PS1 mice fed a normal diet (ND) begin forming major amyloid deposits in the brain at 6 months of age [57–59] and develop memory problems by 9–12 months of age [52, 60, 61]. Therefore, as a pre-onset control, we used 6-month-old Tg mice continuously fed the ND (MF Rations, Oriental Yeast, Japan; its composition is shown in Supplementary Table 1). As a normal aging control, Wt littermates maintained continuously on the ND were used. Until 4 months of age, all of the mice were maintained on the ND. The mice were given free access to water and food. During the HFD feeding period, we changed the food in the cage every 2 days and determined the consumption per cage by measuring the difference in food pellet weight. All of the mice were weighed every other week during the ND or HFD experimental period.

Cholinesterase inhibitor (ChEI) treatment

In a clinical setting, rivastigmine can be administered subcutaneously to AD patients [62]. In a pilot experiment, we administered donepezil intraperitoneally (2 mg/kg/day) [32] as well as rivastigmine by subcutaneous infusion (2 mg/kg/day), into 6-month-old Tg-HFD mice for a week. Donepezil did not show any ameliorative effects, but rivastigmine tended to ameliorate the neuroinflammation and hippocampal neurogenesis compared to non-treated Tg-HFD mice. Therefore, we used rivastigmine as a cholinesterase inhibitor in this study. An Alzet Osmotic Pump 2006 (Alzet, Durect) was implanted subcutaneously into HFD-fed AβPP/PS1 Tg mice at 4.5 months of age. Each mouse was deeply anesthetized with an intramuscular injection of ketamine (50 mg/kg) and xylazine (5 mg/kg), the back was minimally incised under general anesthesia, and a subdermal space was expanded for pump insertion. An Alzet Osmotic Pump 2006 was filled with a rivastigmine solution (2 mg/kg/day) or saline (vehicle) (Otsuka, Japan), the pump was immediately implanted subcutaneously using a sterile instrument, and the cut was sutured. The wound was thoroughly disinfected, and the mouse was warmed on a heating plate (37°C) to maintain body temperature until it recovered from the anesthesia. The implanted pump remained in place until the end of the experiments, and continuously released the solution under the skin for 6 weeks. The solution containers were filled and the osmotic pump was implanted according to the manufacturer's instructions.

Retrovirus-mediated labeling of adult-born neurons

Plat-GP cells and constructs for retroviral vectors that express GFP in new neurons were kindly donated by Dr. K. Inokuchi's laboratory at the University of Toyama, and we produced the retrovirus vector in our laboratory. The virus was prepared essentially as described previously [63]. Briefly, the two constructs, pMXs-SIN-CAG-GFP and pVSV-G, were co-transfected into Plat-GP cells by the calcium phosphate method, and the medium was replaced 12–16 h after transfection to minimize cell damage. After 2-3 days, the culture medium containing the retrovirus was collected, and the retrovirus was concentrated by two consecutive ultracentrifugations, at 50,000 × g for 90 min and 50,000 × g for 90 min, at 4°C. The retroviral pellet was resuspended in phosphate-buffered saline (PBS) to 0.05% of the original volume. The retrovirus was thusly cultured and concentrated for each injection. The virus solution was kept on ice until just before use, when it was injected into the dentate gyrus of 5-month-old mice. For the injection, the mouse was deeply anesthetized by intramuscular injection of a mixed solution of ketamine/xylazine (50/5 mg/kg), and was placed in a stereotactic device. A concentrated GFP-expressing retroviral solution (more than 10^8 infectious units/mL) was stereotactically injected into a single site in the hippocampal dentate gyrus (AP: +2.0 mm posterior; ML: ±1.5 mm lateral; DV: –2.0 mm ventral 1.5 μL/site) at a constant speed (0.5 μL/min). The mouse was placed on a heating plate (37°C) while the wound was sutured, and was kept on the plate to maintain body temperature until it

recovered from the anesthesia. The integration of the retroviral vector into the host genome only occurs in dividing cells, and the cells are permanently labeled with GFP. The mice were sacrificed and examined 4 weeks after the retrovirus injection.

BrdU administration and cell counts

To label newly born cells in 5-month-old mice, bromodeoxyuridine (BrdU, Wako, Japan) was injected into mice intraperitoneally (100 mg/kg in 0.9% saline) for 5 consecutive days (24-h intervals). The animals were sacrificed 4 weeks after the last injection, and the brain was dissected out and fixed. For BrdU immunohistochemistry, a series of every 12th coronal section (480-μm apart) throughout the entire dentate gyrus was processed. All of the BrdU-positive cells in the dentate gyrus (the granule cell layer, including the subgranular zone) were counted under a 100× objective lens by an observer blinded to the experimental conditions. We analyzed 4 sections per mouse and multiplied the number of BrdU-positive cells by 12 to obtain a stereological estimate of the total number of these cells per hippocampal dentate gyrus [32].

Morris water maze (MWM) test

Rivastigmine treatment was stopped when the mice were 6 months old. Nine days before the end of rivastigmine treatment, we assessed spatial learning and memory by subjecting the mice to MWM tests for 6 consecutive days, and to contextual fear conditioning (CFC) tests on the next 3 days. To minimize the confounding effects of anxiety on learning, the mice were handled extensively for 2 min per day for 7 consecutive days prior to beginning the MWM testing [64]. The MWM test was conducted as described previously with some modifications [65]. Briefly, on days 1–5 of MWM testing, the mice were placed in a dimly lit circular pool (120-cm diameter, 35-cm deep) filled with opaque water (23°C ± 1°C) and surrounded by abundant extra-maze distal and visual cues, and were required to arrive at a hidden platform submerged 1 cm below the surface of the water within 60 s. A total of 30 trials (6 trials per day for 5 consecutive days) were performed in the training sessions. In the spatial task, the mice were carefully placed afloat at the edge of the pool, with their face turned toward the pool wall. The starting points were semi-randomly chosen from north (N), east (E), south (S), or west (W), and the escape platform was located in the middle of the SW quadrant. All mice took the test in the same order. In each trial, mice that failed to find the platform within 60 s were guided to the platform and allowed to sit on the platform for 20 s before being picked up. After the initial training, the inter-trial interval was approximately 30 min. Twenty-four hours after the training session, in the last trial (day 6), the escape platform was removed and the mice were allowed to swim for 60 s in the pool starting from the N side (the single-probe trial). The time spent in the target quadrant where the platform was previously located during a single 60-s trial was measured. Just before the first trial each day, the mouse cages were placed in the same condition as the behavioral test for at least 30 min to allow the mice to acclimatize to the experimental field. Mice were warmed on a heating plate (37°C) between trials and after the last trial to prevent hypothermia. All data were recorded and analyzed with the SMART video tracking system (Panlab).

Contextual fear conditioning (CFC) test

On the day following the final day of the MWM tests, the mice were subjected to CFC to evaluate hippocampal-dependent contextual memory and non-hippocampal (amygdala)-dependent cued memory. All equipment and software for the CFC tests were purchased from Med Associates. The testing procedures have been described in detail [48, 66]. In brief, on the first day of CFC testing, mice were placed in a conditioning chamber (30 cm wide × 26 cm deep × 24 cm high). The chamber consisted of a white-lit rectangular room with a stainless steel grid floor (2-mm diameter wire, spaced 5 mm apart) and aluminum and acrylic walls. The chambers were scented with 70% isopropanol. In the acquisition (training) phase of the CFC test, the mice underwent three conditioning trials during a 370-s session under the same conditions, after which an electric shock (1 s, 0.75 mA) was delivered through the floor accompanied by an aural tone (white noise). The tone sounded at 128, 212, and 296 s into the session, lasting for 10 s each time, and the footshock was delivered during the last 1 s of the tone.

Twenty-four hours later, during the second day of CFC, the mice were placed in the same environmental conditions as on the first day for 512 s, and the durations of mouse freezing behavior were measured throughout the session to test context-elicited fear (contextual memory). Neither tones nor shocks were presented.

Twenty-four hours after the contextual memory test, on the third day of CFC testing, the mice were placed into a novel context, and the same tone as on the first day was sounded for 512 s. Freezing times were analyzed throughout the session to test for tone-elicited fear (cued memory) without electroshock. The new context had a red-lit triangular room with a white plastic floor and an acrylic black triangle-frame roof, and was scented with 70% ethanol. The tone began sounding 128 s after the start of the session.

Before the first session each day, the mouse cages were placed in a low-lit, quiet room for at least 30 min to soothe anxiety. All of the sessions were recorded by a video camera attached to the chamber, and the freezing time was automatically calculated with Video Freeze software (Med Associates).

Collection of blood samples and measurement of serum insulin levels

Twenty-four hours after the cognitive experiments were finished, the mice were deeply anesthetized, and their blood was collected from a cardiac vessel immediately prior to perfusion. The blood samples were kept at room temperature for 2 h to promote clotting. The samples were then centrifuged at 4°C for 15 min at 2,320 × *g*. The obtained supernatant serum was carefully aliquoted into several sterile tubes. The samples were stored at –20°C until just before use. The serum insulin levels were measured using a mouse-specific insulin ELISA kit (Morinaga, Japan) following the manufacturer's instructions.

Sandwich ELISA assay

Mice were deeply anesthetized and decapitated, and the hippocampus was immediately dissected out, frozen with liquid nitrogen, and kept at –80°C until homogenization. For homogenization, the frozen hippocampus was thawed and homogenized in ice-cold RIPA buffer containing a cocktail of protease inhibitors (Santa Cruz) using an ultrasonic homogenizer (Tomy Seiko, Japan). The homogenates were centrifuged (100,000 × *g*, 1 h, 4°C), and the aliquoted supernatants were stored at –80°C until their analysis by ELISA (soluble fraction). The remaining pellet was further solubilized in a 5 M guanidine HCl/50 mM Tris HCl solution (pH 8.0) by incubating for 3 h at room temperature, and centrifuged (100,000 × *g*, 1 h, 4°C). The supernatants were aliquoted and kept at –80°C until use (insoluble fraction, guanidine soluble). Protein concentrations for the soluble and insoluble extracts were determined using the BCA protein assay kit (TaKaRa Bio, Japan) according to the manufacturer's instructions. The levels of amyloid-β ($A\beta)_{40}$ and $A\beta_{42}$ in the hippocampus were determined by a sandwich ELISA with Human/Rat (Mouse) $A\beta_{40}$ and $A\beta_{42}$ ELISA Kits (Wako, Japan). The Aβ oligomer levels were measured with the Human Amyloid-β Oligomers (82E1-specific) Assay Kit (IBL, Japan). The levels of IL-1β and TNF-α in the hippocampal supernatants were assayed using mouse IL-1β and TNF-α ELISA Kits (R&D Systems). The hippocampal extracts were appropriately diluted with the diluent buffer to fall within the standard range and applied to the ELISA plates. All ELISA procedures were conducted according to the manufacturer's instructions. The standards and samples were assayed in duplicate at appropriate dilutions. The optical density was analyzed at 450 nm within 30 min of chromogen mixing on a microplate spectrophotometer. Concentrations were calculated according to a standard curve. Data obtained from the hippocampal homogenates are expressed as picomoles of Aβ species per gram of total protein (pmol/g) or as picograms of cytokines per gram of total protein (pg/g), taking into account the dilution factor.

Brain-tissue perfusion

Twenty-four hours after the last day of CFC testing, the mice were deeply anesthetized, and transcardially perfused with ice-cold PBS (pH 7.4) followed by 4% paraformaldehyde (PFA) (pH 7.4). The brain was removed and postfixed in fresh 4% PFA solution at 4°C for 24 h, and then equilibrated in 30% sucrose/PBS solution at 4°C until it sank (3 days). The dehydrated brain was then embedded in Tissue-Tek OCT Compound (Sakura Finetek, Japan) and frozen at –80°C. The frozen brain samples were sliced into 40-μm coronal sections using an HM525 cryostat (Microm, Germany). Brain slices were taken from the entire hippocampus. All slices were submerged in cryoprotectant solution and stored at –20°C until use.

X-34 synthesis and histochemical staining

We used a previously described protocol to organically synthesize X-34 and use it to stain senile plaque [48, 67]. X-34 is a highly fluorescent dye that is derived from Congo Red and specifically

binds amyloid aggregates. Briefly, X-34 was synthesized from tetraethyl p-xylylenediphosphonate (Tokyo Chemical Industry, Japan), 5-formylsalicylic acid (Sigma-Aldrich), and potassium tert-butoxide (Sigma-Aldrich) in our laboratory, and was used in solution. Brain sections were washed 3 times in Tris-buffered saline (TBS), incubated with X-34 solution for 30 min, gently washed by dipping in TBS, and incubated in a 0.2% NaOH/80% ethanol solution for 2 min. The samples were washed again with TBS and incubated with TOTO-3 iodide (Molecular Probes) in TBS to stain the cell nuclei. The samples were then washed with TBS and mounted on microscope slides. Three sections were treated for each animal.

Immunohistochemistry

Brain sections were washed 3 times in TBS or TBS containing 0.3% Triton-X (0.3% TBS-X), then blocked with 3% normal donkey serum (NDS) diluted in 0.3% TBS-X at room temperature for 90 min.

For immunofluorescent BrdU staining, the sections were washed twice and placed in 10 mM citric acid (pH 6.0) at 90°C for 5 min in a water bath for antigen activation. The sections were then cooled at room temperature, rinsed with TBS, incubated in 1 N HCl at 37°C for 30 min, and incubated in boric acid buffer (pH 8.4) at room temperature for 10 min. The sections were then rinsed twice in TBS and incubated in blocking solution at room temperature for 60 min. After blocking, the free-floating sections were incubated with primary antibodies at 4°C for 3 days, washed 3 times with TBS, and incubated with secondary antibodies conjugated with various fluorescent dyes at room temperature for 2 h in light-resistant containers.

Next, the brain sections were washed once with TBS and incubated with 4′6-diamidino-2-phenylindole (DAPI) (1:10000, Sigma) in TBS at room temperature for 5 min. Excess DAPI was removed by washing with TBS, and the sections were mounted on microscope slides with Immu-Mount (Thermo Scientific) and visualized using a confocal microscope.

The primary antibodies used in this study were anti-BrdU rat IgG (1:200, Oxford Biotech), anti-NeuN mouse IgG (1:1000, Millipore), anti-GFAP mouse IgG (1:500, Sigma), anti-ionized calcium-binding adaptor molecule 1 (Iba1) rabbit IgG (1:1000, Wako, Japan), anti-doublecortin (DCX) guinea pig IgG (1:2000, Millipore), and anti-GFP rat IgG (1:1000, Nacalai Tesque), as reported previously [49]. The secondary antibodies used were anti-rat IgG donkey IgG Alexa488 (1:1000, Molecular Probes), anti-mouse IgG donkey IgG Alexa647 (1:1000, Molecular Probes), anti-rabbit IgG donkey IgG Alexa568 (1:1000, Molecular Probes), anti-rabbit donkey IgG Alexa488 (1:1000, Molecular Probes), and anti-guinea pig donkey IgG Cy5 (1:200, Jackson ImmunoResearch). All antibodies were diluted in 0.3% TBS-X containing 3% NDS. For DCX immunostaining, three sections were measured for each mouse.

Confocal microscopy and cell quantification

Sections stained with X-34 were analyzed with a confocal microscope (TCS SP2; Leica, Germany) using a 40× oil-immersion objective lens. Fluorescence immunostaining was quantified using a confocal microscope with a 20× (GFAP/Iba1), 40× (DCX), or 100× (BrdU/Iba1 and BrdU/NeuN) oil-immersion objective lens. Images were displayed in the maximum-intensity projection of a z-series stack acquired at 1.0-μm intervals throughout 40-μm-thick sections. For the confocal imaging of dendritic spines, we used a 63× oil-immersion objective lens with a 2.0× optical zoom at 0.5-μm step intervals (z-stack).

To count GFAP+ or Iba1+ cells in the hippocampus, immunofluorescence images were taken from three consecutive coronal sections per mouse, from Bregma –1.70 to –2.10 mm, spaced 0.2 mm apart. GFAP+ and Iba+ cells in the hippocampus were manually counted from digitalized confocal images in the hippocampal areas, and were averaged per section.

For the analyses of dendritic spine density and the maturity of newborn neurons, GFP-labeled spines were divided into four subtypes according to their morphology. During the process of synaptogenesis, a mature spine (mushroom and thin spine), which has a neck and head, is known to be derived from immature finger-like protrusions (filopodia) and stubby spines [43, 68, 69]. Thus, in this study, all of the GFP+ spines were categorized and quantified manually as immature type or mature type based on these criteria.

Dendritic growth of DCX+ neurons

The maturity of doublecortin (DCX)-immunopositive granule cells was evaluated as previously described [70, 71]. In the morphological analysis, all of the DCX-positive (+) cells in the dentate gyrus were manually classified as immature or mature according to their dendritic growth pattern. As newborn DCX+ granule cells mature, they

gradually project dendrites toward the molecular layer, and the dendrites develop more and more complex branches.

In our analysis, DCX+ cells located adjacent to the subgranular zone (SGZ) and having bipolar neurites parallel to the SGZ, or having primary dendrites that did not extend beyond the middle of the granule cell layer, were considered immature. DCX-reactive cells in the SGZ with long dendrites projecting toward and crossing the molecular layer were considered to be mature. Only DCX+ cells with sharply defined cell bodies were assessed for maturity.

Image processing

Images of X-34 staining were obtained by confocal microscopy and analyzed with ImageJ software as described previously [48]. Briefly, the outer edge of the hippocampal area was manually designated into regions-of-interest, and the percentage of the area containing senile plaque, which was labeled with X-34 fluorescence, was automatically calculated using a plug-in. This process was applied to each section to determine the proportion of amyloid load in the hippocampus.

Statistical analyses

Data are presented as means ± SEM of the number of biological replicates (as noted in the figure legends). All data were analyzed for significant differences by one-way ANOVA followed by Dunnett's or Williams's multiple-comparison *post hoc* test (one group served as a control), by a Chi-squared test, and by a non-paired two-tailed Student's *t*-test for two groups (placebo group, AD-Vehicle mice versus treatment group, AD-Rivastigmine mice). We considered $p < 0.05$ to be statistically significant.

RESULTS

Lack of influence of rivastigmine on the diabetic pathology of T2DM-AD model mice

In this study, we used T2DM-AD model mice fed a high-fat diet (HFD) for 2 months (Tg-HFD) [48]. Our previous study [48] revealed that the Tg-HFD mice show early-onset amnesia, so we used the Tg-HFD mice as AD model mice. As a normal aging control and pre-onset control, we used wild-type (Wt) littermate and Tg mice fed a normal diet (ND), respectively. At the end of the experimental period, despite similar food consumption in the two groups (Fig. 1A, B; ND-fed group versus HFD-fed group), the HFD-fed mice weighed about 1.5 times more than the ND-fed mice (Fig. 1C). Rivastigmine treatment had no significant effect on the food intake or body weight. The HFD-fed mice gradually accumulated fat and became obese, but had no other behavioral abnormalities in their cages. Rivastigmine is reported to carry a risk of appetite loss for some AD patients [15]; however, we did not observe any significant difference in feeding behavior in the rivastigmine-treated mice. Even after the surgery to implant the osmotic pump, the mice quickly resumed their normal dietary habits.

As shown in Fig. 1D, HFD-fed mice had significantly higher serum insulin levels, an important indicator of type 2 diabetes mellitus (T2DM), compared with ND-fed mice (one-way ANOVA, $F_{(3,31)} = 11.0, p < 0.01$; AD-Vehicle mice, $n = 8$, Dunnett's *post hoc* test, compared with AD-Vehicle: Wt-ND, $n = 8$, $^{**}p < 0.01$; Tg-ND, $n = 8$, $^{**}p < 0.01$). Rivastigmine did not noticeably affect these high insulin levels. Thus, all of the HFD-fed mice developed the T2DM pathophysiology, regardless of whether they were treated with rivastigmine or the control solution.

Rivastigmine suppresses glial neuroinflammatory responses in T2DM-AD model mice

We evaluated neuroinflammatory reactions in the brain of the T2DM-AD model mice fed the HFD for 2 months, by immunohistochemistry and ELISA. Figure 2 shows the results of immunostaining for astrocytes (GFAP) and microglia (Iba1) in the hippocampus of each group. This analysis showed that the inflammation-related glial cells were activated in the hippocampus of the T2DM-AD model mice (AD-Vehicle), as indicated by their intense staining and high cell density, whereas normal control mice (Wt-ND) showed more sparse astrocytes and microglia (Fig. 2A). Rivastigmine treatment suppressed the glial inflammatory responses compared to the AD-Vehicle group. Notably, rivastigmine effectively inhibited the high concentration and hypertrophy of astrocytes and microglia around microaggregates composed of enlarged glial cells, which surrounded senile plaques (Supplementary Figure 1), in these T2DM-AD model mice.

Quantitative analyses revealed that there were significantly more astrocytes and microglia, including reactive hypertrophied cells, in the hippocampus of the AD-Vehicle group compared to that of

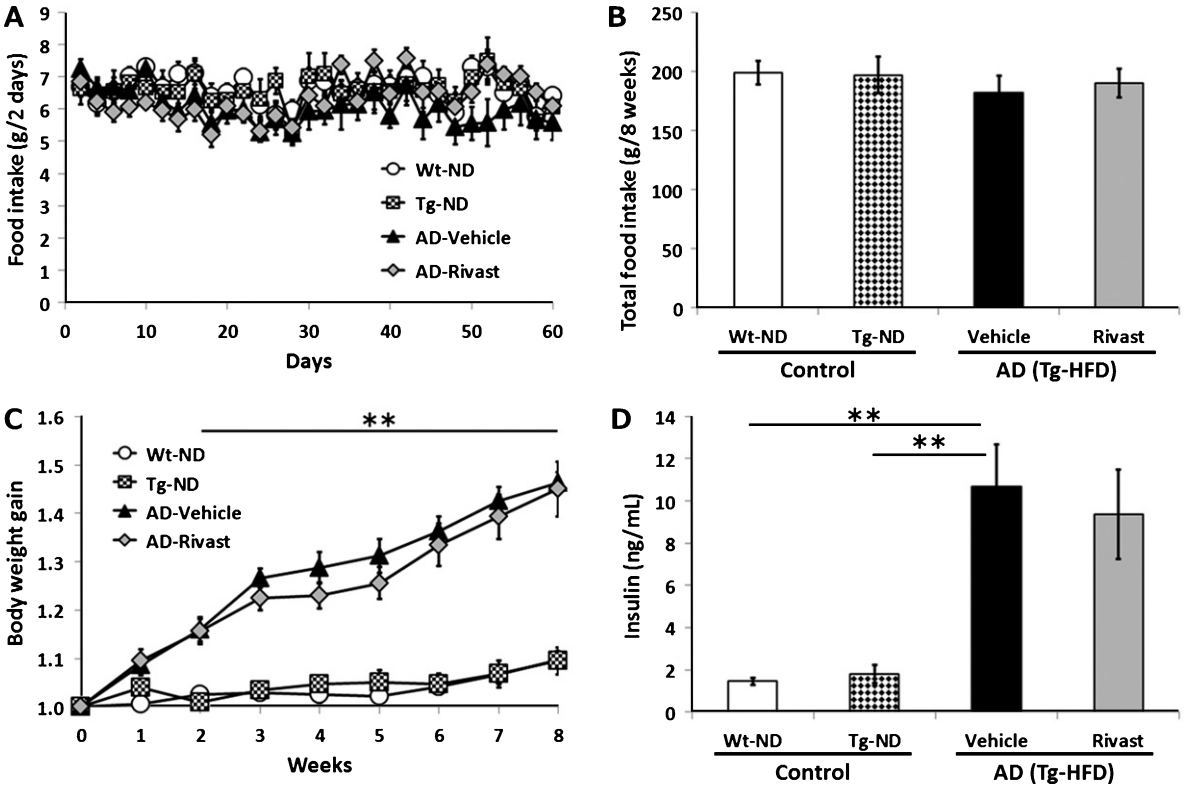

Fig. 1. Rivastigmine does not affect metabolic changes in the T2DM-AD model mice. A) Transitional changes in average dietary intake every 2 days for each group. B) Total food intake in the food intervention period (8 weeks) before sacrifice. Rivastigmine treatment through an implanted subcutaneous pump did not affect ingestive behavior. C) Body-weight changes. Data represent the ratio of the weight at each experimental point to the weight at 4 months of age. HFD-fed mice had gained significantly more body weight than ND-maintained mice despite commensurate food consumption. The final body weight of the HFD-fed mice was approximately 1.5 times that of ND-fed mice. Administering rivastigmine through an osmotic pump did not markedly influence the body weight. D) Serum insulin levels in each group of mice. The two HFD-fed groups had abnormally high serum insulin levels compared with the two ND-fed groups. Rivastigmine did not significantly change the concentration of serum insulin. Data represent the mean ± SEM; $n = 8$ per group; $^{**}p < 0.01$, Dunnett's multiple-comparison test (control: AD-Vehicle). Wt, wild-type; Tg, AβPP/PS1 transgenic; ND, normal diet; HFD, high-fat diet; Rivast, rivastigmine.

the Wt control (Fig. 2B, C; GFAP+ cells, one-way ANOVA, $F_{(3,15)} = 16.0$, $p < 0.01$; AD-Vehicle mice, $n = 4$, Dunnett's *post hoc* test, compared with AD-Vehicle: Wt-ND, $n = 4$, $^{**}p < 0.01$; Tg-ND, $n = 4$, $^{**}p < 0.01$; Iba1+ cells, one-way ANOVA, $F_{(3,15)} = 5.14, p < 0.05$; AD-Vehicle mice, $n = 4$, Dunnett's *post hoc* test, compared with AD-Vehicle: Wt-ND, $n = 4$, $^{**}p < 0.01$). Neuroinflammation was not induced by the HFD alone, as we did not detect a significant increase in the number of activated glial cells in the Wt-HFD versus the Wt-ND hippocampus (Supplementary Figure 2).

We found that rivastigmine treatment suppressed neuroinflammation in these T2DM-AD model mice. Importantly, rivastigmine treatment suppressed the increased number of GFAP+ astrocytes in the hippocampus of the AD-Vehicle mice (Fig. 2B, AD-Rivastigmine, $n = 4$, $^{**}p < 0.01$). Rivastigmine treatment also caused a significant decrease in the number of Iba1+ microglia ($^{*}p < 0.05$) (Fig. 2C). To clarify the effect of rivastigmine on the activation of microglial cells, we also quantified the number of newly born microglia in the hippocampus [72, 73]. As shown in Fig. 3, we detected a significant decrease in the number of double-positive (BrdU+/Iba1+) cells in the AD-Rivastigmine group, compared with that in the AD-Vehicle group (Fig. 3, $^{*}p < 0.05$). Collectively, these results indicated that severe inflammation, which appeared as strong microglial generation, occurred in the AD-Vehicle mice, and that rivastigmine significantly inhibited this cellular inflammatory response.

Chronic neuroinflammation is mediated by proinflammatory cytokines. ELISAs revealed that the levels of IL-1β and TNF-α were significantly increased in the hippocampus of AD-Vehicle mice, and that

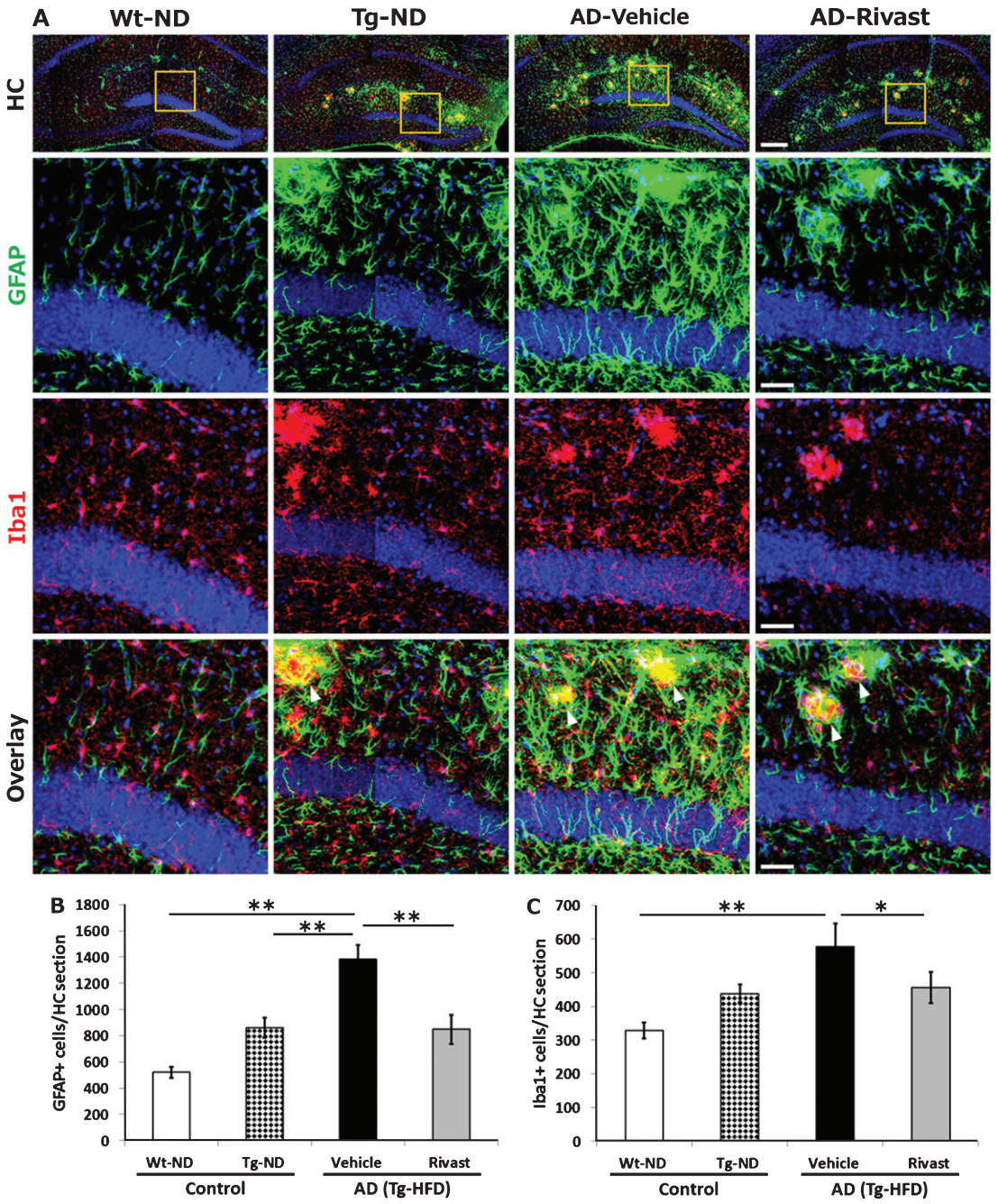

Fig. 2. Rivastigmine suppresses the exacerbated gliosis in the hippocampus of T2DM-AD mice. A) Representative images of hippocampal sections triple stained for GFAP (green), Iba1 (red), and DAPI (blue). The lower panels show magnified views. Activated astrocytes and microglia characteristically exhibited an expanded volume and high population density. The GFAP-labeled astrocytes and Iba1-labeled microglia were noticeably activated in the hippocampus of AD-Vehicle mice. In contrast, the hippocampus of AD-Rivastigmine mice showed predominantly small astrocytes and microglia, as in Wt-ND mice, in particular near the cellular aggregates of glial cells. White arrowheads indicate microaggregates of activated astrocytes and microglia, which surrounded senile plaques. Scale bar, 50 μm. B) Average number of GFAP-immunopositive cells per coronal section in the hippocampus. Astrocytes were significantly denser in the hippocampus of AD-Vehicle mice than in that of ND-fed Wt or Tg mice, and the increased astrocyte accumulation was markedly decreased by rivastigmine. C) Average number of Iba1-immunopositive cells per coronal section in the hippocampus. Significantly more microglia accumulated in the hippocampus of AD-Vehicle mice compared to that of Wt-ND mice, and rivastigmine significantly decreased the elevated microglial population. Data represent the mean ± SEM; $n = 4$ per group; $^{**}p < 0.01$, $^{*}p < 0.05$, Dunnett's or Williams' multiple-comparison test (control: AD-Vehicle). HC, hippocampus; Wt, wild-type; Tg, AβPP/PS1 transgenic; ND, normal diet; HFD, high-fat diet; Rivast, rivastigmine.

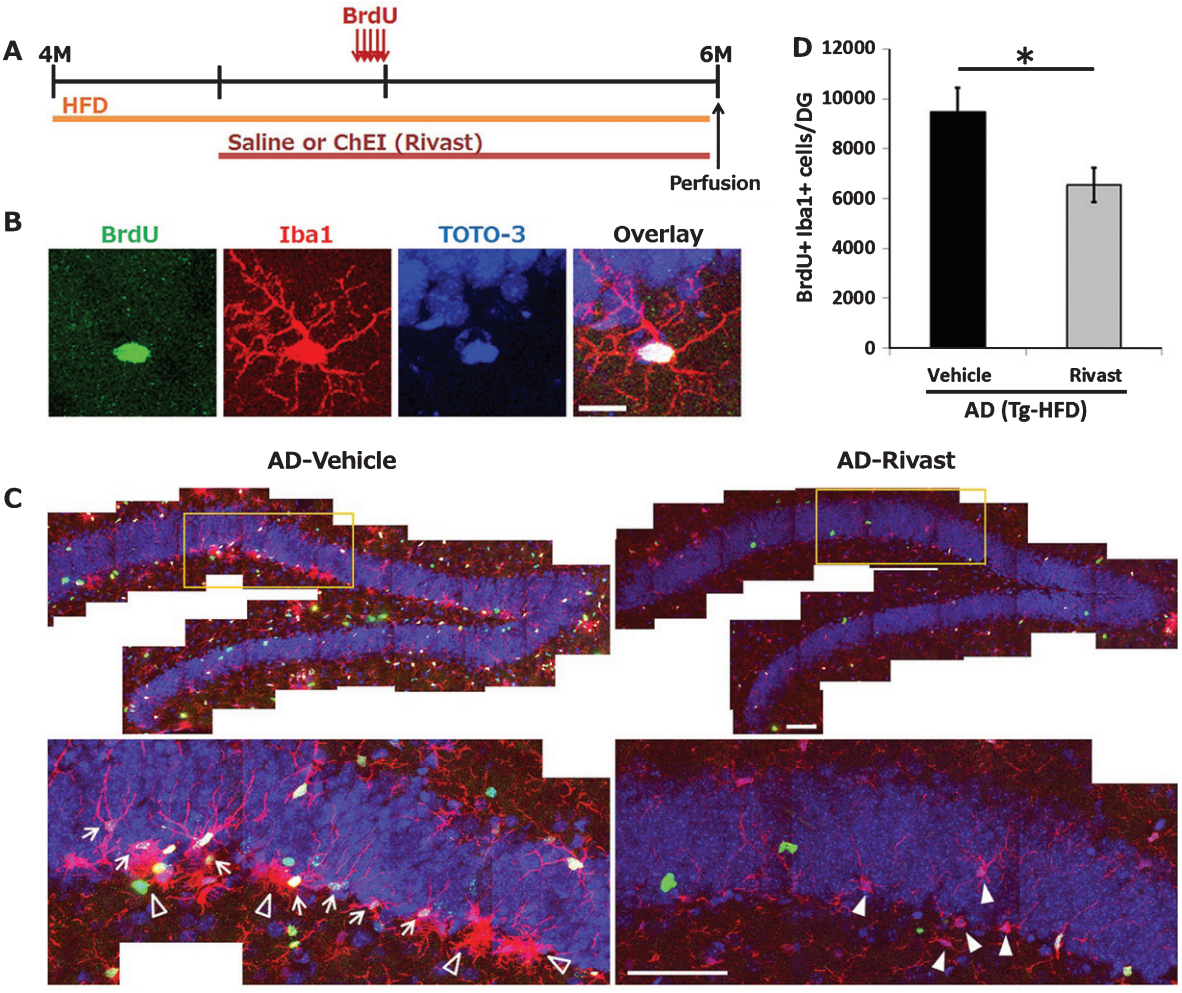

Fig. 3. Rivastigmine decreases the proliferation of microglial cells in T2DM-AD mice. A) Experimental time line. Microglial proliferation directly reflects the microenvironmental neuroinflammation. Thus, we labeled and quantified newly generated microglia by BrdU. B) Confocal microscopy images of cells in the granule cell layer (GCL) labeled with BrdU (green), Iba1 (red), and TOTO-3 (blue), showing typical BrdU+/Iba1+/TOTO-3+ cells (newborn microglia). Scale bar, 10 μm. C) Representative images of the hippocampal dentate gyrus of AD-Vehicle and AD-Rivastigmine mice. The lower panels show magnified views. Hypertrophied reactive microglia located in the dentate subgranular zone were rapidly dividing in vehicle-treated AD mice, while most of the cells in the rivastigmine-treated AD mice were static, ramified microglia. The arrows and white-outlined arrowheads indicate BrdU+/Iba1+ newborn microglia and hyperactive microglial aggregates, respectively (left panel). White arrowheads indicate BrdU-negative/Iba1-positive (BrdU–/Iba1+) quiescent microglia (right panel). Scale bar, 50 μm. D) Quantitative analysis of the newborn microglia. There were significantly more BrdU+/Iba1+ cells in the dentate gyrus of vehicle-treated AD mice than in that of rivastigmine-treated AD mice. Data represent the mean ± SEM; $n = 5$ per group. $^{*}p < 0.05$, two-tailed unpaired Student's *t*-test. Tg, AβPP/PS1 transgenic; HFD, high-fat diet; ChEI, cholinesterase inhibitor; Rivast, rivastigmine.

rivastigmine substantially decreased these levels (Fig. 4) (IL-1β, one-way ANOVA, $F_{(3,15)} = 7.60$, $p < 0.01$; AD-Vehicle mice, $n = 4$, Dunnett's *post hoc* test, compared with AD-Vehicle: Wt-ND, $n = 4$, $^{*}p < 0.05$; AD-Rivastigmine, $n = 4$, $^{**}p < 0.01$; TNF-α, one-way ANOVA, $F_{(3,15)} = 6.64$, $p < 0.01$; AD-Vehicle mice, $n = 4$, Dunnett's *post hoc* test, compared with AD-Vehicle: Wt-ND, $n = 4$, $^{**}p < 0.01$; AD-Rivastigmine, $n = 4$, $^{**}p < 0.01$). These results indicated that AβPPswe/PSEN1dE9 AD model mice fed the HFD for 2 months (AD-Vehicle group) develop elevated proinflammatory cytokine levels, and that rivastigmine treatment affects not only cellular, but also molecular inflammatory responses.

Rivastigmine does not prevent the amyloid pathology of T2DM-AD model mice

We also analyzed the amyloid pathology in each group of mice. First, we measured the senile plaque

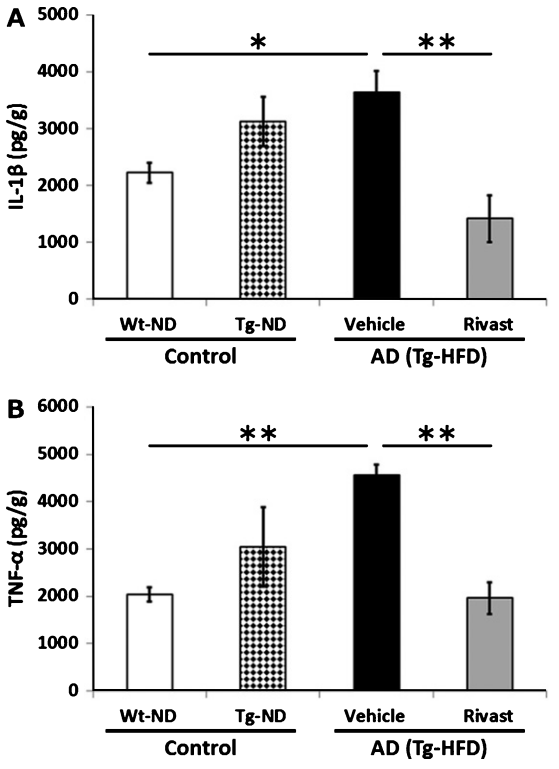

Fig. 4. Elevated proinflammatory cytokine levels in the T2DM-AD mice are reduced by rivastigmine. IL-1β (A) and TNF-α (B) levels in hippocampal extracts. The levels of these proinflammatory cytokines were significantly increased in the AD-Vehicle mice, and rivastigmine effectively decreased them. Data are displayed as picograms of cytokines per gram of total protein (pg/g). Data represent the mean ± SEM; $n = 4$ per group; $^{**}p < 0.01$, $^{*}p < 0.05$, Dunnett's multiple-comparison test (control: AD-Vehicle mice).

load in the hippocampus by histochemical labeling with X-34. Figure 5A shows representative images of X-34 staining in each group of mice. The percent area (Fig. 5B) and number of senile plaques (Fig. 5C) in both the vehicle-treated (AD-Vehicle) and rivastigmine-treated (AD-Rivastigmine) AD model mice was comparable to that in the pre-onset control mice (Tg-ND). These results indicated that ingesting large amounts high-fat food does not alter amyloid deposition during the experimental food period, and that rivastigmine does not beneficially influence the amount of amyloid plaque accumulation.

Second, we investigated by ELISA the levels of three types of soluble Aβ peptides ($A\beta_{40}$, $A\beta_{42}$, and Aβ oligomers), which are more toxic than insoluble peptides, in the hippocampus. Compared to normal control mice (Wt-ND), the levels of all of the Aβ peptide types were markedly elevated in all three groups of AβPP/PS1 mice, and rivastigmine did not significantly decrease them (Fig. 5D-F). Interestingly, AD-Vehicle mice produced significantly more $A\beta_{42}$ than Tg-ND mice (Fig. 5E; one-way ANOVA, $F_{(3,15)} = 13.5$, $p < 0.01$; AD-Vehicle mice, $n = 4$, Dunnett's *post hoc* test, compared with AD-Vehicle: Tg-ND, $n = 4$, $^{*}p < 0.05$). We also performed ELISAs for the insoluble Aβ species, which showed no significant differences among the three groups of Tg mice (Fig. 5G-I). These results suggested that long-term HFD feeding increases the soluble $A\beta_{42}$ in the hippocampus of the Tg mice, but this increase is not blocked by rivastigmine treatment.

Rivastigmine ameliorates the memory decline in T2DM-AD model mice

To assess rivastigmine's effect on cognitive decline in the T2DM-AD model mice, we subjected the mice to MWM and CFC tests, both of which involve hippocampal-dependent memory tasks (Figs. 6 and 7). We used four groups of mice in these behavioral tests; in addition to the AD-Vehicle mice (placebo group) and AD-Rivastigmine mice (treatment group), their littermate Wt and Tg mice fed ND were used as control groups.

In the MWM tests, spatial learning and memory was evaluated in both an acquisition phase (days 1–5) and a probe trial (day 6). In the acquisition phase of the MWM test, we observed significant differences in memory function between the normal control (Wt-ND) and the AD-Vehicle group during the training period, but did not observe any significant difference between the AD-Vehicle and the AD-Rivastigmine mice (Fig. 6A, B). In the single-probe trial on day 6, the memory performance was significantly impaired in the AD-Vehicle mice compared with the normal control (Wt-ND) mice, and this cognitive decline was averted in the AD-Rivastigmine mice (Fig. 6C, D; one-way ANOVA, $F_{(3,31)} = 7.50$, $p < 0.01$; AD-Vehicle mice, $n = 8$, Dunnett's *post hoc* test, compared with AD-Vehicle: Wt-ND, $n = 8$, $^{**}p < 0.01$; AD-Rivastigmine, $n = 8$, $^{**}p < 0.01$). In the single-probe test, most of the mice in the placebo group failed to enter the target quadrant, indicating that they did not retain the spatial memory. In contrast, mice from the rivastigmine-treated group often entered the target quadrant where the hidden platform had been placed during the training sessions.

The same sets of mice were next subjected to CFC tests. On the first day, the mice were trained with a conditioning task. On the second day, we evaluated the hippocampal-dependent memory

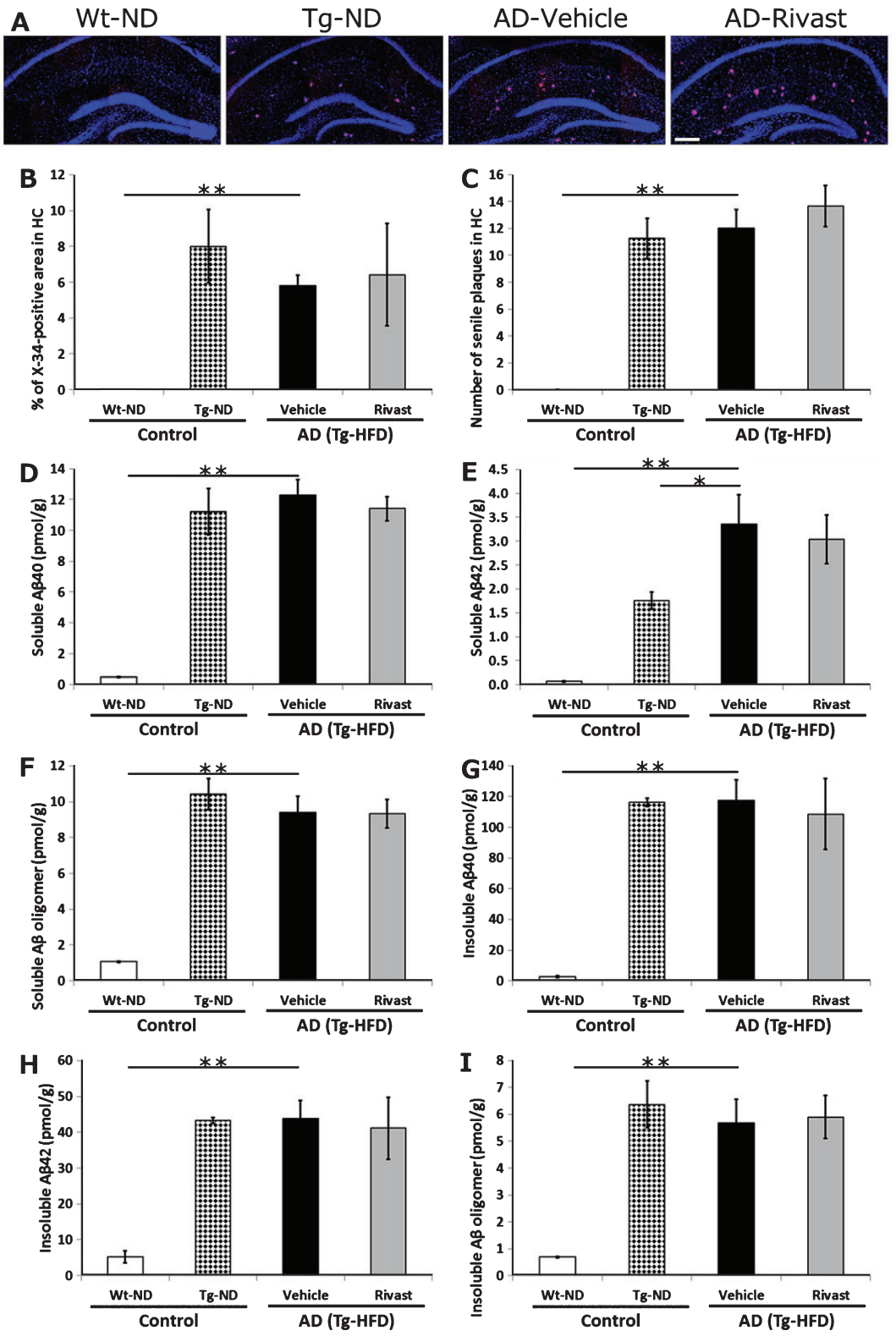
A
Wt-ND
Tg-ND
AD-Vehicle
AD-Rivast
B
% of X-34-positive area in HC
C
Number of senile plaques in HC
D
Soluble Aβ40 (pmol/g)
E
Soluble Aβ42 (pmol/g)
F
Soluble Aβ oligomer (pmol/g)
G
Insoluble Aβ40 (pmol/g)
H
Insoluble Aβ42 (pmol/g)
I
Insoluble Aβ oligomer (pmol/g)
Wt-ND
Tg-ND
Vehicle
Rivast
Control
AD (Tg-HFD)

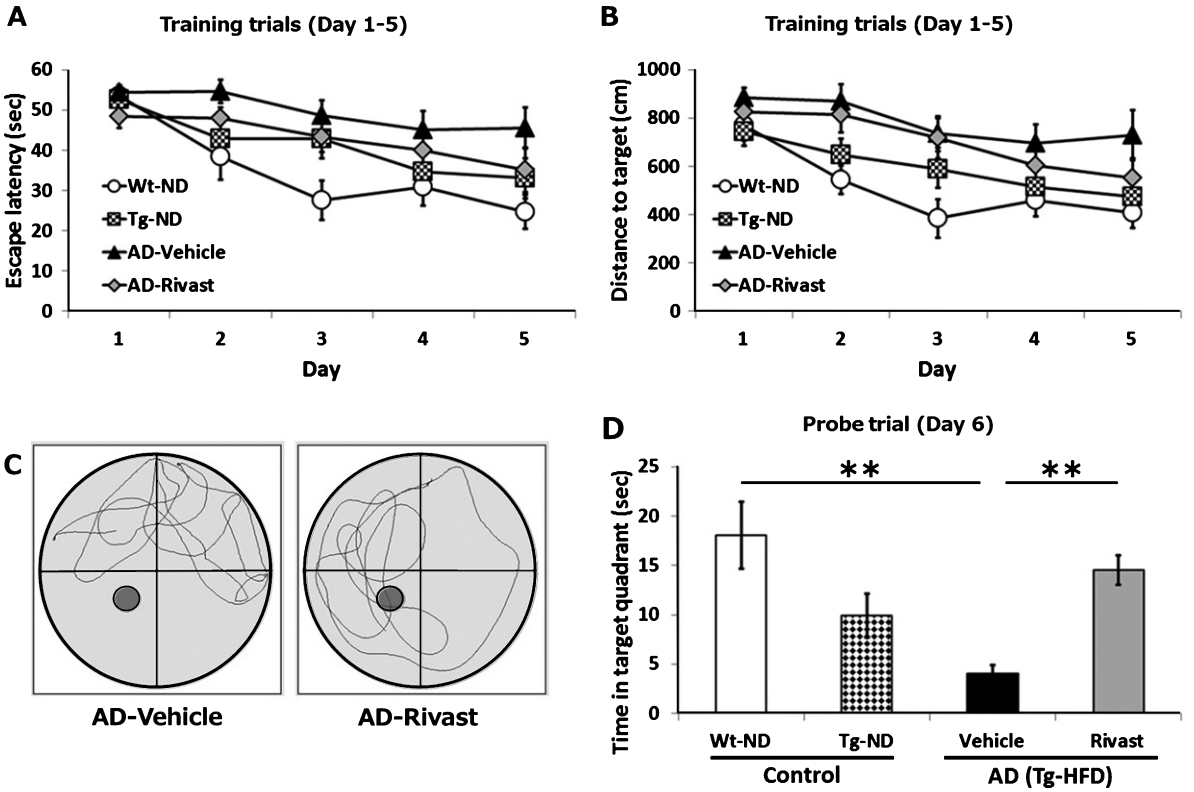

Fig. 6. Rivastigmine ameliorates the deterioration of long-term memory. Learning and memory functions were evaluated by the Morris water maze (MWM) test at both the acquisition phase to assess short-term memory (days 1–5, ITI: 30 min) and the retrieval phase to measure long-term memory (day 6, ITI: 24 h). A) Escape latency during training sessions on days 1–5. Significant differences were observed between Wt-ND and AD-Vehicle mice on days 2, 3, and 5, but rivastigmine did not influence the memory performance. B) Distance to target during training trials on days 1–5. No locomotive or motivational abnormalities were observed in any group of mice. C) Representative computer-generated tracing of the swim of an AD-Vehicle (left) versus AD-Rivastigmine (right) mouse in the probe test. D) Time in the target quadrant in a single-probe trial on day 6. Notably, the staying time of the AD-Vehicle mice in the target quadrant was significantly shorter than that of the Wt-ND mice, while AD-Rivastigmine mice maintained the same memory function as the Wt-ND mice. MWM tests revealed that the both the short-term and long-term memory in HFD-fed Tg mice were impaired and that rivastigmine recovered the deficit in long-term memory. Data represent the mean ± SEM; $n = 8$ per group; $^{**}p < 0.01$, Dunnett's multiple-comparison test (control: AD-Vehicle). ITI, inter trial interval; Wt, wild-type; Tg, AβPP/PS1 transgenic; ND, normal diet; HFD, high-fat diet; Rivast, rivastigmine.

performance in each group by measuring their freezing time. We found that rivastigmine treatment significantly improved the ability of the AD model mice to perform this hippocampal-dependent memory task (Fig. 7A, B; one-way ANOVA, $F_{(3,31)} = 9.00$, $p < 0.01$; AD-Vehicle mice, $n = 8$, Dunnett's *post hoc* test, compared with AD-Vehicle: Wt-ND, $n = 8$, $^{**}p < 0.01$; AD-Rivastigmine, $n = 8$, $^{**}p < 0.01$). We

Fig. 5. Rivastigmine does not affect the senile plaque or soluble Aβ production. A) Representative images of senile plaques in the hippocampus (HC), stained by X-34, for each group of mice. No amyloid load was observed in Wt-ND mice. The amyloid deposits were similar in the three Tg groups. Scale bar, 50 μm. B) Measurement of the Aβ burden in the mouse hippocampus. The percentage of the hippocampal region that was labeled by X-34 is shown for each type of mouse. There was no significant difference in the amount of amyloid burden in the hippocampus of vehicle (control)- and rivastigmine-treated AD mice. C) The number of senile plaques in a hippocampal slice. There was no marked difference in plaque numbers among the three types of Tg mice. D) Level of soluble $A\beta_{40}$ in hippocampal homogenates. E) Level of soluble $A\beta_{42}$ in hippocampal lysates. ELISAs showed that the HFD significantly increased the $A\beta_{42}$ production in Tg mice, and rivastigmine did not alter this production. F) Level of soluble Aβ oligomers. Oligomer levels in soluble brain fractions were determined using an ELISA specific for aggregated/oligomeric Aβ. No significant difference was observed in the level of Aβ oligomers in vehicle-treated and rivastigmine-treated T2DM-AD mice. G) Level of insoluble $A\beta_{40}$ in hippocampal homogenates. H) Level of insoluble $A\beta_{42}$ in hippocampal lysates. I) Level of insoluble Aβ oligomers. No significant differences were observed in the amount of insoluble Aβs in the hippocampus of the three groups of Tg mice. Data from ELISA assays are displayed as picomoles of Aβ species per gram of total protein (pmol/g). Data represent the mean ± SEM; $n = 4$ per group; $^{**}p < 0.01$, $^{*}p < 0.05$, Dunnett's multiple-comparison test (control: AD-Vehicle). Wt, wild-type; Tg, AβPP/PS1 transgenic; ND, normal diet; HFD, high-fat diet; Rivast, rivastigmine.

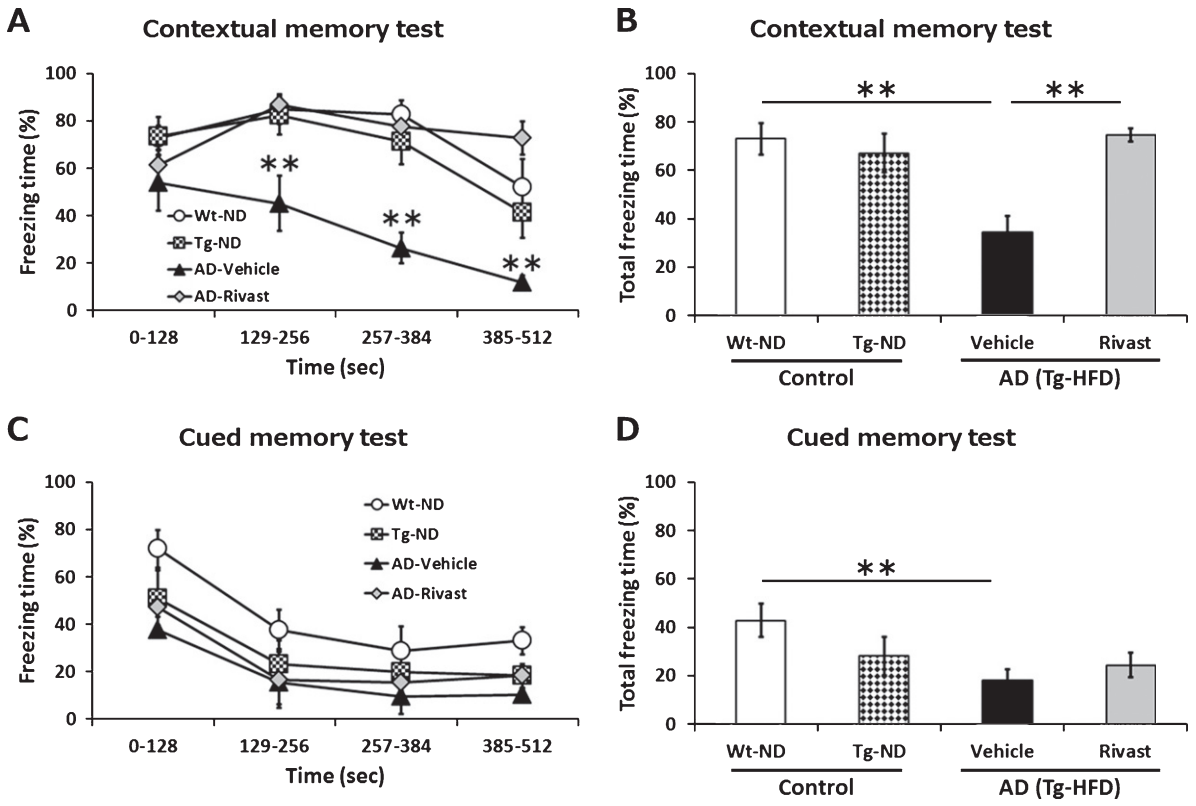

Fig. 7. Rivastigmine prevents the impairment of hippocampal-dependent memory. In the contextual fear conditioning (CFC) test, mice were subjected to both a contextual memory test to assess hippocampal-dependent memory and a cued memory test to measure amygdala-dependent memory. A) Transitional freezing time in the contextual memory test. Significant differences were observed between the AD-Vehicle mice and the other groups of mice ($^{**}p < 0.01$). B) Total freezing time in the contextual memory test. Vehicle-treated AD mice had significant contextual memory defects, and the defects were ameliorated in the rivastigmine-treated AD mice. C) Transitional freezing time in the cued memory test. The performance of AD-Vehicle mice was impaired compared to Wt-ND mice. D) Total freezing time in the cued memory test. Tg-HFD-Saline mice performed poorly in this test ($^{**}p < 0.01$), and rivastigmine did not significantly improve their performance. These CFC tests revealed that the rivastigmine-treated AD mice retained their hippocampal-dependent spatial memory, which was equivalent to that of Wt-ND mice, while vehicle-treated AD mice failed to learn the task. Data represent the mean ± SEM; $n = 8$ per group; $^{**}p < 0.01$, Dunnett's multiple-comparison test (control: AD-Vehicle mice). Wt, wild-type; Tg, AβPP/PS1 transgenic; ND, normal diet; HFD, high-fat diet; Rivast, rivastigmine.

also measured the freezing time of the mice in the tone fear-conditioning test on the following day, which showed that the cued memory was impaired in the AD-Vehicle mice. Rivastigmine had no detectable effect on this impairment (Fig. 7C, D). These results indicated that rivastigmine effectively prevents the decline in the hippocampal-dependent, but not amygdala-dependent, memory performance of the 6-month-old T2DM-AD model mice.

Rivastigmine reverses the retarded hippocampal neurogenesis in T2DM-AD model mice

Next, we compared the level of adult hippocampal neurogenesis among the four groups; Wt-ND, Tg-ND, AD (Tg-HFD)-vehicle, and AD (Tg-HFD)-rivastigmine. To count the number of new neurons in the hippocampus, we injected BrdU into these mice ($n = 5$ in each group) 5 times at 5 months of age, and examined their brains 4 weeks later. Figure 8 shows the quantification of BrdU-positive and NeuN-positive (BrdU+/NeuN+) cells in the dentate gurus of the four groups. Surprisingly, immunostaining showed that BrdU+/NeuN+ cells were markedly increased in the two groups of T2DM-AD mice (AD-Vehicle and AD-Rivastigmine) compared with normal control (Wt-ND) mice (one-way ANOVA, $F_{(3,19)} = 4.16$, $p < 0.05$; Williams' *post hoc* test, compared with Wt-ND: AD-Rivastigmine and AD-Vehicle, $^{*}p < 0.05$).

To evaluate the maturation of the new neurons in the two T2DM-AD mouse groups (AD-Vehicle

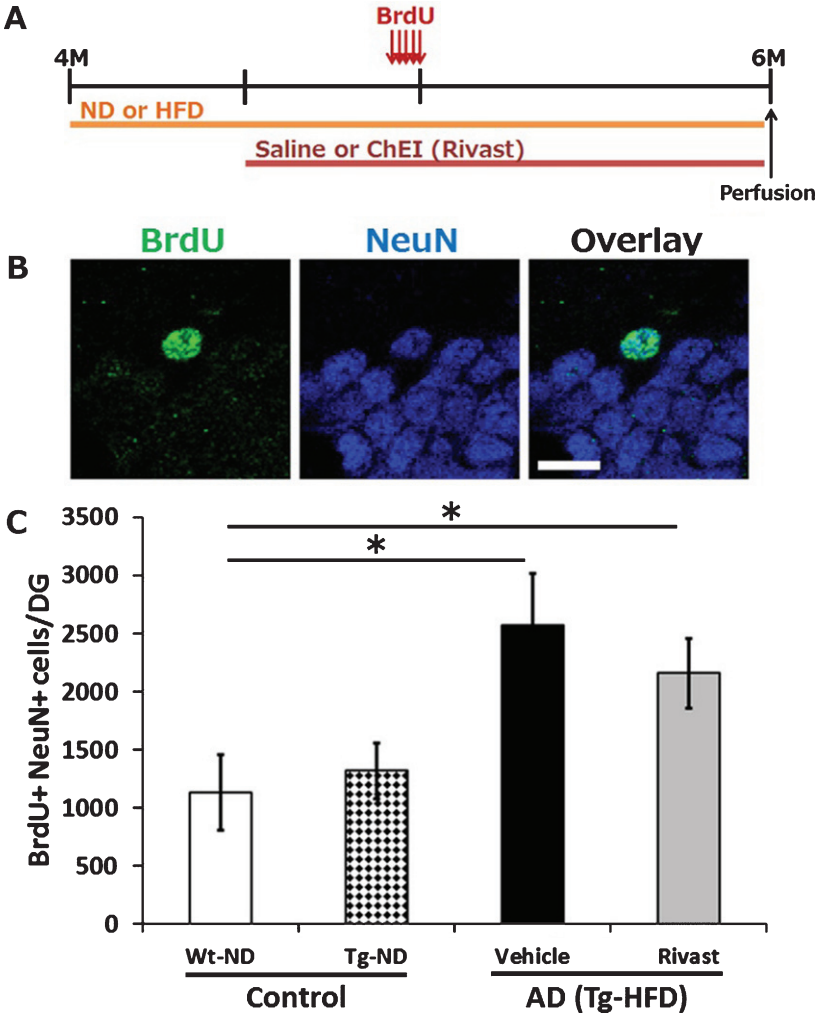

Fig. 8. Increased number of hippocampal newborn neurons in T2DM-AD model mice. A) Timeline of the experimental design. B) Immunofluorescent images showing the co-expression of BrdU (Green) with the neuronal marker NeuN (Blue). Scale bar, 10 μm. C) Quantification of BrdU+/NeuN+ cells in the dentate gyrus. Unexpectedly, the number of dividing newborn neurons in the dentate gyrus of AD-Vehicle mice was significantly larger than that in Wt-ND mice. Rivastigmine did not appear to affect this upregulation. Data represent the mean ± SEM; $n = 5$ per group. $^{*}p < 0.05$, Williams' multiple-comparison test (control: Wt-ND). DG, dentate gyrus; Wt, wild-type; Tg, AβPP/PS1 transgenic; ND, normal diet; HFD, high-fat diet; ChEI, cholinesterase inhibitor; Rivast, rivastigmine.

and AD-Rivastigmine), we performed immunohistochemistry for doublecortin (DCX) [70, 71]. Figure 9A shows the qualitative analysis of DCX-positive (DCX+) cells, which are newly born neuroblasts and immature neurons. For the morphological analysis, DCX+ cells in the dentate gyrus were classified into immature cells or mature cells according to their dendritic pattern (Fig. 9B), and the percentage of mature DCX+ cells in each group was quantified (Fig. 9C). Statistical analysis showed a clear decrease in the percentage of mature DCX+ cells in the AD-Vehicle group, whereas the AD-Rivastigmine group maintained the same percentage of mature DCX+ cells as that seen in the normal control group (Wt-ND) (one-way ANOVA, $F_{(3,11)} = 6.49$, $p < 0.05$; Dunnett's *post hoc* test, compared with AD-Vehicle: Wt-ND, $^{*}p < 0.05$; AD-Rivastigmine, $^{*}p < 0.05$). These results suggested that rivastigmine effectively reverses the retarded maturation of new neurons in the AD model mice.

To further assess the effect of rivastigmine treatment to reverse the retarded maturation of new neurons in the AD model mice, we analyzed the maturity of dendritic spines using a retroviral GFP labeling method. In this experiment, we labeled the hippocampal spines in 5-month-old mice by a

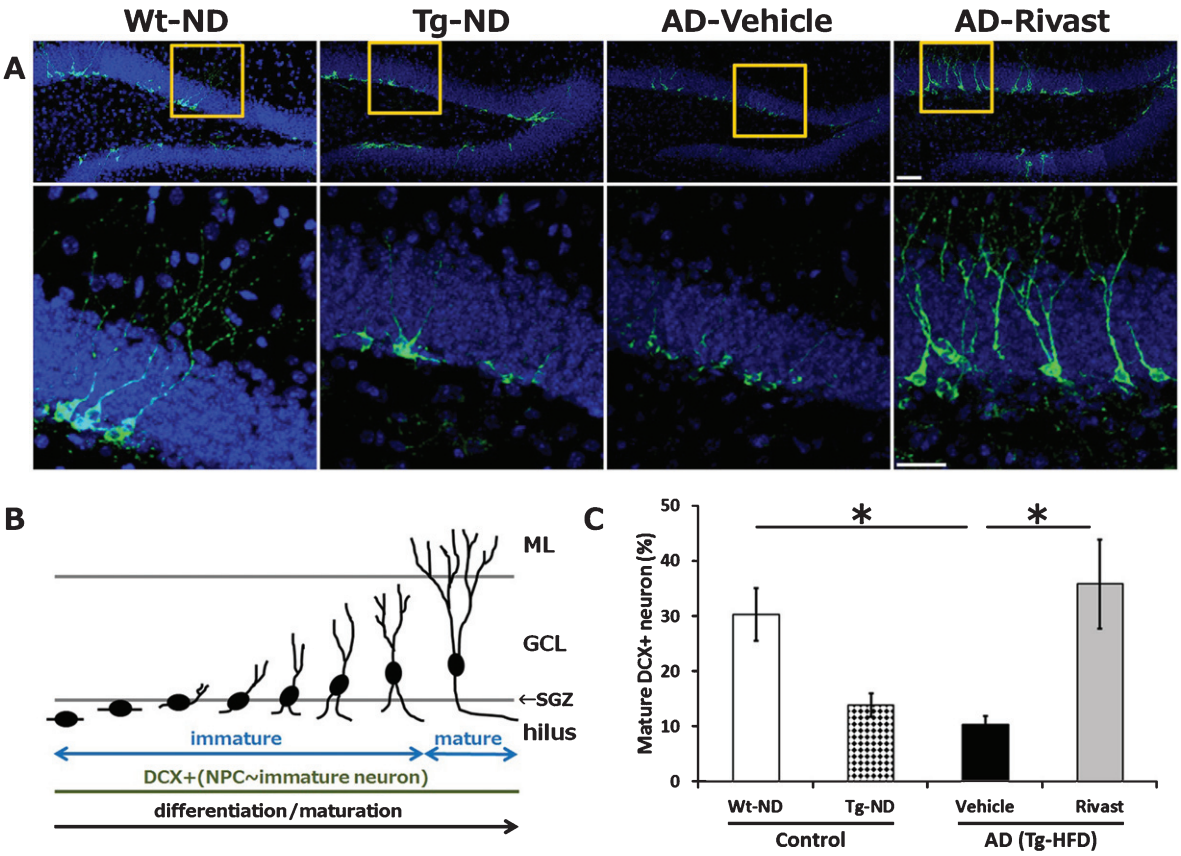

Fig. 9. Rivastigmine improves the maturation of newborn granule cells. The phenotype of adult-born neurons under inflamed conditions was investigated by immunostaining for the neural progenitor/immature neuron marker doublecortin (DCX). A) Representative images of DCX (green) and DAPI (blue) immunostaining in the subgranular zone (SGZ) of the dentate gyrus, showing that DCX-positive (+) neurons in AD-Vehicle mice had extremely short primary dendrites. In contrast, the primary dendrites in the Wt-ND and AD-Rivastigmine mice extended into the molecular layer (ML) at a right angle to the SGZ. Scale bar, 50 μm. B) Schematic illustration of the development of newborn granule cells in the SGZ. DCX+ cells were categorized as immature or mature according to the length of their primary dendrites. All of the DCX+ cells in the dentate gyrus were manually identified and counted according to these criteria. C) Percentage of mature DCX+ neurons among all DCX+ neurons in the dentate gyrus. The percentage of mature DCX+ cells was significantly reduced in AD-Vehicle mice, and the mature DCX+ cell count was recovered by rivastigmine treatment. These results suggest that the maturation process of young neurons is inhibited in vehicle-treated AD mice and is restored by rivastigmine. Data represent the mean ± SEM; $n = 3$ per group. $^{*}p < 0.05$, Dunnett's multiple-comparison test (control: AD-Vehicle). DCX, doublecortin; SGZ, subgranular zone; ML, molecular layer; GCL, granule cell layer; NPC, neural progenitor cell; Wt, wild-type; Tg, AβPP/PS1 transgenic; ND, normal diet; HFD, high-fat diet; Rivast, rivastigmine.

retrovirus, and examined their brains 4 weeks later (Fig. 10A). The GFP-labeled spines of 4-week-old neurons were classified as immature type (filopodia and stubby) and mature type (thin or mushroom-shaped) (Fig. 10B). Confocal observation revealed that the development of dendrite complexity and the formation of spines in newly born neurons were significantly impaired in the AD-Vehicle mice compared with normal control mice (Wt-ND) (Fig. 10C, D). Intriguingly, rivastigmine treatment ameliorated this aberrant spine formation. In addition, quantitative analysis showed that there were significantly fewer GFP+ spines in the AD-Vehicle mice than in Wt-ND mice, and that rivastigmine restored the spine density (Fig. 10E; Total spines/10 μm: one-way ANOVA, $F_{(3,32)} = 39.04$, $p < 0.01$; Dunnett's *post hoc* test, compared with AD-Vehicle: Wt-ND, $^{**}p < 0.01$; AD-Rivastigmine, $^{**}p < 0.01$). Classification of these GFP+ spines revealed that there was a statistically lower percentage of mature spines in the new neurons of AD-Vehicle mice compared with Wt-ND and AD-Rivastigmine mice (Fig. 10E, $^{**}p < 0.01$). These findings suggested that the development of dendritic spines in the AD-Vehicle mice was severely damaged by inflammatory responses, and that rivastigmine treatment noticeably prevented this neuroinflammation-related dysfunction in the maturation of newborn neurons.

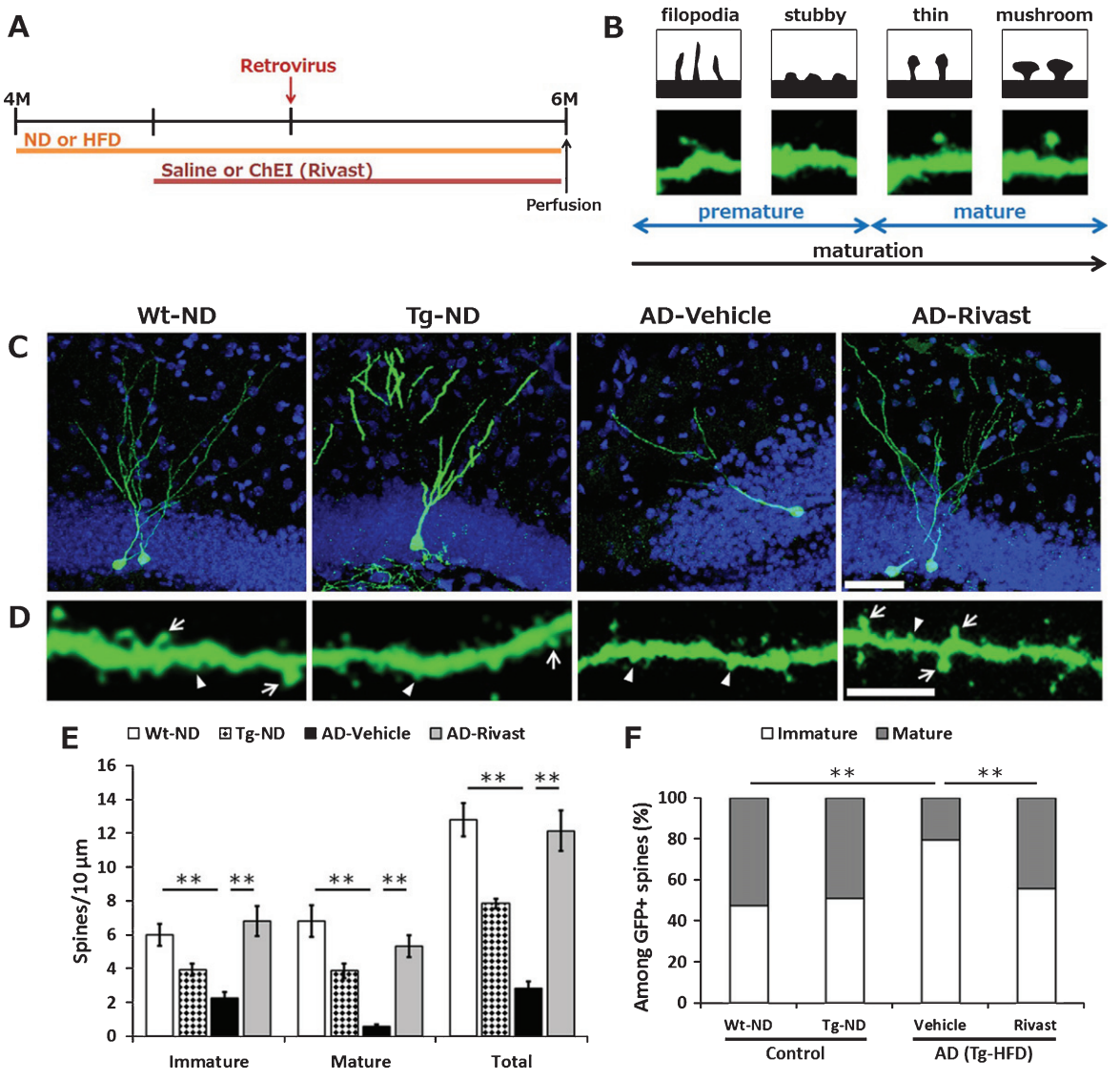

Fig. 10. Rivastigmine recovers the formation of spines in newly born neurons. A) Timeline of the experiment. A GFP-expressing retroviral vector was injected into the hippocampus of each mouse, and the mouse was sacrificed 4 weeks later. Dividing cells in the hippocampus were infected with the infused retrovirus and were labeled with GFP. B) Schematic diagram illustrating the spine maturation process. GFP-positive (+) spines were categorized as immature or mature based on their morphology. Newly generated spines typically shift from immature headless spines to mature enlarged-head spines during their development. C) Representative confocal images of GFP+ newborn neurons in the dentate gyrus. Rivastigmine-treated AD mice and Wt-ND mice had complex dendrites with long branches. Vehicle-treated AD mice had shorter dendrites. Scale bar, 50 μm. D) Representative photographs of GFP+ dendritic spines in the dentate gyrus. White arrowheads indicate immature filopodia and stubby spines; white arrows indicate mature mushroom-shaped and thin spines. The maturation of dendritic spines on newly generated neurons was disturbed in the AD-Vehicle mice. In contrast, the dendritic spines in AD-Rivastigmine mice matured comparably to those in Wt-ND mice. Scale bar, 5 μm. E) Quantitative analysis of the spine morphology in vehicle control or rivastigmine-treated AD mice. Left panel, GFP+ neurons of AD-Rivastigmine mice exhibited significantly more spines than those of AD-Vehicle mice. Data indicate the average number of dendritic protrusions per 10 μm of dendrites from four mice in each group. Data represent the mean ± SEM; Wt-ND N = 128, Tg-ND $N = 141$, AD-Vehicle $N = 51$ spines, AD-Rivastigmine $N = 334$ spines. One-way ANOVA followed by Dunnett's multiple-comparison test (control: AD-Vehicle), $^{**}p < 0.01$. F) Histogram showing that the percentage of mature spines in rivastigmine administrated AD mice was significantly greater than that in the AD-Vehicle group. Chi-squared test, $^{**}p < 0.01$, *post hoc* test, $^{**}p < 0.01$. Wt, wild-type; Tg, AβPP/PS1 transgenic; ND, normal diet; HFD, high-fat diet; ChEI, cholinesterase inhibitor; Rivast, rivastigmine.

These results pertaining to adult hippocampal neurogenesis suggested that in the T2DM-AD model mice, neuroinflammation strongly retards the maturation of newly born granule cells with respect to both dendrite and spine morphogenesis, and in response to this maturation defect, the number of newborn neurons markedly increases, mainly to compensate for the absence of structurally and functionally mature newly born neurons. Moreover, our results indicate that rivastigmine recovers the maturation, but not the proliferative activity, of newborn neurons predominantly by reducing the severe neuroinflammatory responses in the T2DM-AD model mice.

DISCUSSION

In the present study, we discovered that cholinergic modulation by 6 weeks of rivastigmine treatment suppresses glial neuroinflammation and recovers the maturation of new neurons in the hippocampus of T2DM-AD model mice. Rivastigmine, a broad-spectrum cholinesterase inhibitor widely used to treat AD in clinical practice, not only upregulates ACh levels [22] but also acts as an anti-inflammatory agent [25, 26] by inhibiting both AChE and BChE [74, 75]. Importantly, we found that rivastigmine treatment suppressed the amnesia occurring in the T2DM-combined AD model mice, which results from the interaction of an amyloid pathology and HFD-induced neuronal damage [48].

Rivastigmine blocked the elevation of neuroinflammatory reactions in this AD-model mouse, including the activation of microglia and astrocytes and the enhanced production of proinflammatory cytokines IL-1β and TNF-α in the hippocampus, but did not affect the amyloid pathology or insulin metabolism in this mouse. Furthermore, rivastigmine treatment reversed the retarded dendritic maturation of hippocampal new neurons in this mouse by reducing the neuroinflammatory reactions near the neurogenic region. Based on these collective findings, we hypothesize that cholinesterase inhibitors including rivastigmine prevent the memory decline occurring in early AD patients as well as AD model mice, mainly by reducing neuroinflammatory reactions, and not by attenuating the amyloid or insulin pathology.

To our great surprise, we detected an increase in the number of new neurons in the T2DM-combined AD model mice. Indeed, there are a few reports showing enhanced neurogenesis in AD model mice under certain conditions [37–41], but most studies using various AD model mice have shown a convincing down-regulation of hippocampal neurogenesis in AD [34–36]. Verret et al. reported that the survival of new neurons is impaired in AβPPswe/PSEN1dE9 transgenic mice, the same transgenic strain used in the present study [34]. The difference between our current study and the one by Verret et al. is in the dietary conditions. In our study, in addition to senile plaque accumulation, the AβPPswe/PSEN1dE9 transgenic mice developed a T2DM-like pathology, including hyperinsulinemia and brain vascular lesions due to their HFD, as we reported previously [48]. Regarding the tau pathology, in a preliminary experiment, we also stained brain sections with the AT8 antibody, but we did not detect any pathological lesions of hyperphosphorylated tau in our T2DM-combined AD model mice (data not shown). In this pathological condition, we detected a significant increase in the number of newly born neurons in the non-treated T2DM-combined AD model mice (AD-Vehicle group) compared with age-matched wild-type littermates. More importantly, we observed that the number of new neurons in the rivastigmine-treated group was almost twice that in the Wt control, and that rivastigmine supported the neuronal maturation of new neurons to the same level seen in the normal control. Therefore, we speculate that rivastigmine treatment potentiates the activity of adult hippocampal neurogenesis even in AD patients.

Our results indicated that rivastigmine recovered the decline of hippocampal-dependent long-term memory observed in the T2DM-combined AD model mice. The memory impairment in 6-month-old AβPPswe/PSEN1dE9 transgenic mice is induced only by chronic HFD feeding, given that the memory function of 6-month-old ND-fed AβPPswe/PSEN1dE9 transgenic mice was equivalent to that of normal control (Wt-ND) mice, as we described before [48]. From these results, the phenotype of the 6-month-old HFD-fed AβPPswe/PSEN1dE9 transgenic mice can be regarded as an AD pathophysiology that initially provokes memory deficits that are further accelerated by the T2DM pathology. Intriguingly, in a preliminary observation, subcutaneous rivastigmine treatment for 6 weeks did not noticeably ameliorate the hippocampal memory disorder of 18-month-old AβPPswe/PSEN1dE9 mice fed the ND (data not shown), in accordance with the observation that cholinesterase inhibitors have limited effects on late-stage AD patients. These results may indicate that rivastigmine influences the AD pathology in a stage-specific or pathology-specific manner.

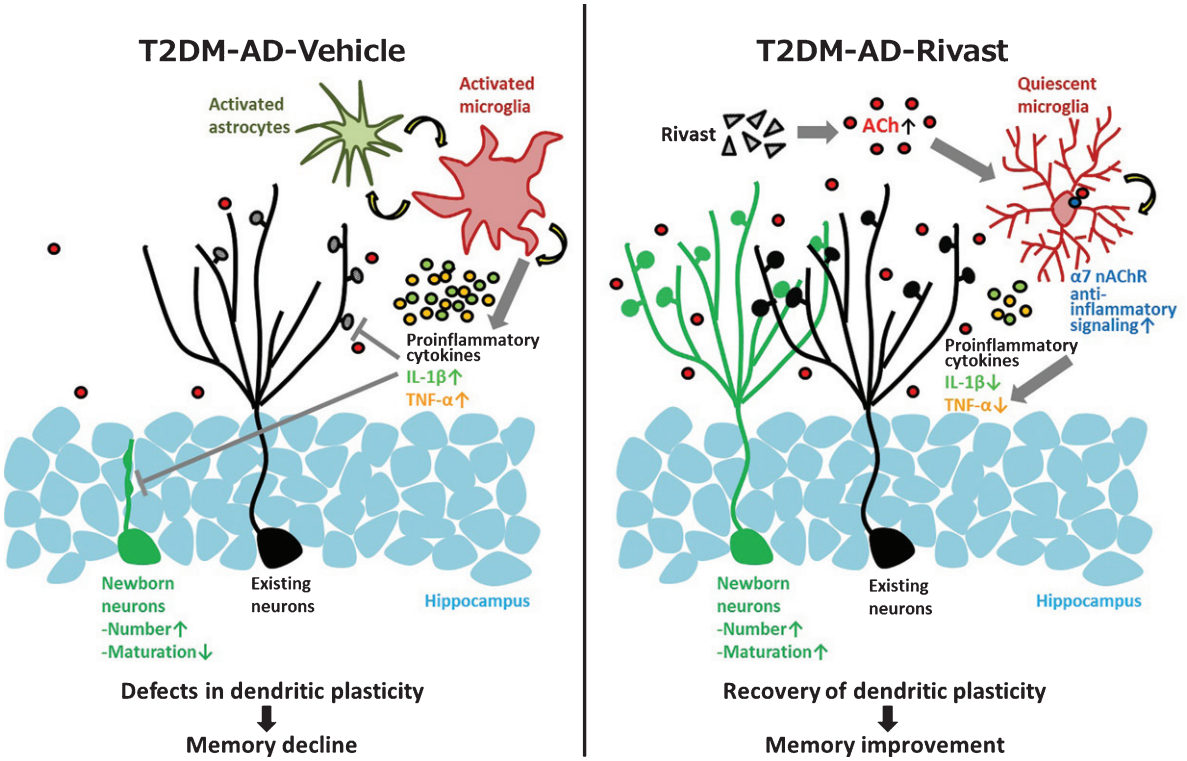

Fig. 11. Schematic illustration of the pathology in the hippocampus of T2DM-AD model mice. Illustration of our hypothetical mechanisms for memory decline in T2DM-AD-Vehicle mice and memory improvement by cholinergic modification in T2DM-AD-Rivastigmine mice. Left) In T2DM-AD-Vehicle mice, gliosis (astrocytes activation and microglial proliferation) are exacerbated, and the production of proinflammatory cytokines (IL-1β and TNF-α) is elevated (Figs. 2–4). Moreover, hippocampal-dependent spatial memory is impaired as shown by two-memory tests: the Morris water-maze and contextual fear conditioning (Figs. 6, 7). The number of new neurons (BrdU+/NeuN+ cells) is enhanced in the dentate gyrus (Fig. 8), but their dendritic maturation is severely abrogated (Figs. 9, 10), suggesting that the gross function of the new neurons in total is severely lower than that in wild-type littermates. The defects in dendritic plasticity in both young and mature hippocampal neurons, as described in earlier studies [43, 78, 80], are likely to be the main reason for the memory impairment in the T2DM-AD model mouse. Right) In T2DM-AD-Rivastigmine mice, neuroinflammatory reactions (gliosis and proinflammatory cytokine production) are suppressed (Figs. 2–4), possibly by anti-inflammatory signaling in microglia through α7 nAChR [94], because rivastigmine treatment upregulates the acetylcholine concentration at extra-synaptic sites, as shown in many previous studies [75, 86–90]. The dendritic plasticity of young and mature hippocampal neurons (Figs. 8–10) and memory performance (Figs. 6, 7) are reversed by rivastigmine to the same levels seen in wild-type mice. Rivastigmine treatment does not change the insulin abnormality or amyloid pathology in this T2DM-AD model mouse (Figs. 1, 5). By this putative scheme, rivastigmine treatment may also prevent the progression of amnesia in AD patients.

The fundamental mechanism of the memory decline occurring in the 6-month-old T2DM-AD model mice is not yet completely understood. Figure 11 is a conceptual diagram illustrating our hypothesis for memory impairment and recovery of the T2DM-AD model mice from our study. In the present study, we observed that the formation of newborn dendritic spines was retarded in the memory-impaired AD model mice, as reported by Richetin et al. [43]. In AD, synaptic deterioration is currently thought to occur early in the disease as a prodromal symptom, and to worsen as the disease advances [76]. A series of reports clearly showed that the spines of existing hippocampal neurons are deteriorated in AD model mice, and that this synaptic dysfunction is a major reason for the memory decline of these mice [77–80]. Recent studies have suggested that proinflammatory cytokines such as IL-1β or TNF-α impair the structural plasticity of dendritic spine formation [81–83].

It has been reported that cholinesterase inhibitors reduce the level of brain inflammatory cytokines such as IL-1β and TNF-α [29, 84, 85]. Rivastigmine treatment upregulates the level of extra-synaptic acetylcholine [75, 86–90]. A type of nAChR, α7 nAChR, is expressed on microglia [91–94], and its activation in microglia decreases the production of proinflammatory cytokines [95]. Our data suggest that rivastigmine, which elevates the ACh level, may work by enhancing α7 nAChR signaling,

triggering an anti-inflammatory process. Taken together, these findings support our hypothesis that a neuroinflammatory response occurs in the hippocampus of T2DM-AD model mice and rivastigmine effectively suppresses this inflammatory reaction to rescue dendritic spine formation, which is required for memory formation.

Our results clearly demonstrate that in the first stages of memory loss in a mouse model of AD combined with T2DM, neuroinflammation promotes gliosis and disturbs neurogenesis in the hippocampus. However, we still need to identify the specific molecules and circuits that regulate the cholinergic events mediating the neuroinflammatory reactions in this AD model mouse. Our findings imply that the cognition of early-stage AD patients might be manipulated and maintained by pharmacological intervention including cholinergic modulation.

ACKNOWLEDGMENTS

This study was financially supported by a JSPS KAKENHI Grant-in-Aid for Scientific Research (Grant No. 25115004) and by Novartis Pharma K.K. to TH. TM was financially supported by the Iwadare Scholarship Foundation. The funding bodies had no role in the design of the study, the collection, analysis, or interpretation of data, or in the writing of the manuscript. The authors acknowledge Ms. Marie Hori for technical assistance, and Prof. Kaoru Inokuchi (University of Toyama, Japan) for providing retroviral vector constructs. Rivastigmine was provided by Novartis Pharma AG.

Authors' disclosures available online (http://j-alz.com/manuscript-disclosures/16-0761r1).

SUPPLEMENTARY MATERIAL

The supplementary material is available in the electronic version of this article: http://dx.doi.org/10.3233/JAD-160761.

REFERENCES

[1] Bachman DL, Wolf PA, Linn R, Knoefel JE, Cobb J, Belanger A, D'Agostino RB, White LR (1992) Prevalence of dementia and probable senile dementia of the Alzheimer type in the Framingham Study. *Neurology* **42**, 115-119.

[2] Ferri CP, Prince M, Brayne C, Brodaty H, Fratiglioni L, Ganguli M, Hall K, Hasegawa K, Hendrie H, Huang Y, Jorm A, Mathers C, Menezes PR, Rimmer E, Scazufca M, Alzheimer's Disease International (2005) Global prevalence of dementia: A Delphi consensus study. *Lancet* **366**, 2112-2117.

[3] Mrak RE, Griffin WS (2007) Common inflammatory mechanisms in Lewy body disease and Alzheimer disease. *J Neuropathol Exp Neurol* **66**, 683-686.

[4] Griffin WS (2013) Neuroinflammatory cytokine signaling and Alzheimer's disease. *N Engl J Med* **368**, 770-771.

[5] Heneka MT, Carson MJ, El Khoury J, Landreth GE, Brosseron F, Feinstein DL, Jacobs AH, Wyss-Coray T, Vitorica J, Ransohoff RM, Herrup K, Frautschy SA, Finsen B, Brown GC, Verkhratsky A, Yamanaka K, Koistinaho J, Latz E, Halle A, Petzold GC, Town T, Morgan D, Shinohara ML, Perry VH, Holmes C, Bazan NG, Brooks DJ, Hunot S, Joseph B, Deigendesch N, Garaschuk O, Boddeke E, Dinarello CA, Breitner JC, Cole GM, Golenbock DT, Kummer MP (2015) Neuroinflammation in Alzheimer's disease. *Lancet Neurol* **14**, 388-405.

[6] Heppner FL, Ransohoff RM, Becher B (2015) Immune attack: The role of inflammation in Alzheimer disease. *Nat Rev Neurosci* **16**, 358-372.

[7] Ott A, Stolk RP, van Harskamp F, Pols HA, Hofman A, Breteler MM (1999) Diabetes mellitus and the risk of dementia: The Rotterdam Study. *Neurology* **53**, 1937-1942.

[8] Peila R, Rodriguez BL, Launer LJ, Study H-AA (2002) Type 2 diabetes, APOE gene, and the risk for dementia and related pathologies: The Honolulu-Asia Aging Study. *Diabetes* **51**, 1256-1262.

[9] Matsuzaki T, Sasaki K, Tanizaki Y, Hata J, Fujimi K, Matsui Y, Sekita A, Suzuki SO, Kanba S, Kiyohara Y, Iwaki T (2010) Insulin resistance is associated with the pathology of Alzheimer disease: The Hisayama study. *Neurology* **75**, 764-770.

[10] Ohara T, Doi Y, Ninomiya T, Hirakawa Y, Hata J, Iwaki T, Kanba S, Kiyohara Y (2011) Glucose tolerance status and risk of dementia in the community: The Hisayama study. *Neurology* **77**, 1126-1134.

[11] Hokama M, Oka S, Leon J, Ninomiya T, Honda H, Sasaki K, Iwaki T, Ohara T, Sasaki T, LaFerla FM, Kiyohara Y, Nakabeppu Y (2014) Altered expression of diabetes-related genes in Alzheimer's disease brains: The Hisayama study. *Cereb Cortex* **24**, 2476-2488.

[12] van Dijk G, van Heijningen S, Reijne AC, Nyakas C, van der Zee EA, Eisel UL (2015) Integrative neurobiology of metabolic diseases, neuroinflammation, and neurodegeneration. *Front Neurosci* **9**, 173.

[13] Bozluolcay M, Andican G, Firtina S, Erkol G, Konukoglu D (2016) Inflammatory hypothesis as a link between Alzheimer's disease and diabetes mellitus. *Geriatr Gerontol Int* **16**, 1161-1166.

[14] Doody RS (1999) Clinical profile of donepezil in the treatment of Alzheimer's disease. *Gerontology* **45**(Suppl 1), 23-32.

[15] Birks J, Grimley Evans J, Iakovidou V, Tsolaki M (2000) Rivastigmine for Alzheimer's disease. *Cochrane Database Syst Rev*, CD001191.

[16] Tariot P (2001) Current status and new developments with galantamine in the treatment of Alzheimer's disease. *Expert Opin Pharmacother* **2**, 2027-2049.

[17] Lilienfeld S (2002) Galantamine–a novel cholinergic drug with a unique dual mode of action for the treatment of patients with Alzheimer's disease. *CNS Drug Rev* **8**, 159-176.

[18] Rösler M, Anand R, Cicin-Sain A, Gauthier S, Agid Y, Dal-Bianco P, Stähelin HB, Hartman R, Gharabawi M (1999) Efficacy and safety of rivastigmine in patients with

Alzheimer's disease: International randomised controlled trial. *BMJ* **318**, 633-638.

[19] Forette F, Anand R, Gharabawi G (1999) A phase II study in patients with Alzheimer's disease to assess the preliminary efficacy and maximum tolerated dose of rivastigmine (Exelon). *Eur J Neurol* **6**, 423-429.

[20] Farlow M, Anand R, Messina J, Hartman R, Veach J (2000) A 52-week study of the efficacy of rivastigmine in patients with mild to moderately severe Alzheimer's disease. *Eur Neurol* **44**, 236-241.

[21] Van Dam D, Abramowski D, Staufenbiel M, De Deyn PP (2005) Symptomatic effect of donepezil, rivastigmine, galantamine and memantine on cognitive deficits in the APP23 model. *Psychopharmacology (Berl)* **180**, 177-190.

[22] Hartmann J, Kiewert C, Duysen EG, Lockridge O, Greig NH, Klein J (2007) Excessive hippocampal acetylcholine levels in acetylcholinesterase-deficient mice are moderated by butyrylcholinesterase activity. *J Neurochem* **100**, 1421-1429.

[23] Rao AA, Sridhar GR, Das UN (2007) Elevated butyrylcholinesterase and acetylcholinesterase may predict the development of type 2 diabetes mellitus and Alzheimer's disease. *Med Hypotheses* **69**, 1272-1276.

[24] Kamal MA, Tan Y, Seale JP, Qu X (2009) Targeting BuChE-inflammatory pathway by SK0506 to manage type 2 diabetes and Alzheimer disease. *Neurochem Res* **34**, 2163-2169.

[25] Darreh-Shori T, Vijayaraghavan S, Aeinehband S, Piehl F, Lindblom RP, Nilsson B, Ekdahl KN, Långström B, Almkvist O, Nordberg A (2013) Functional variability in butyrylcholinesterase activity regulates intrathecal cytokine and astroglial biomarker profiles in patients with Alzheimer's disease. *Neurobiol Aging* **34**, 2465-2481.

[26] Lane RM, Darreh-Shori T (2015) Understanding the beneficial and detrimental effects of donepezil and rivastigmine to improve their therapeutic value. *J Alzheimers Dis* **44**, 1039-1062.

[27] Egea J, Buendia I, Parada E, Navarro E, León R, Lopez MG (2015) Anti-inflammatory role of microglial alpha7 nAChRs and its role in neuroprotection. *Biochem Pharmacol* **97**, 463-472.

[28] Echeverria V, Yarkov A, Aliev G (2016) Positive modulators of the α7 nicotinic receptor against neuroinflammation and cognitive impairment in Alzheimer's disease. *Prog Neurobiol* **144**, 142-157.

[29] Nizri E, Irony-Tur-Sinai M, Faranesh N, Lavon I, Lavi E, Weinstock M, Brenner T (2008) Suppression of neuroinflammation and immunomodulation by the acetylcholinesterase inhibitor rivastigmine. *J Neuroimmunol* **203**, 12-22.

[30] Shifrin H, Nadler-Milbauer M, Shoham S, Weinstock M (2013) Rivastigmine alleviates experimentally induced colitis in mice and rats by acting at central and peripheral sites to modulate immune responses. *PLoS One* **8**, e57668.

[31] Ide Y, Fujiyama F, Okamoto-Furuta K, Tamamaki N, Kaneko T, Hisatsune T (2008) Rapid integration of young newborn dentate gyrus granule cells in the adult hippocampal circuitry. *Eur J Neurosci* **28**, 2381-2392.

[32] Itou Y, Nochi R, Kuribayashi H, Saito Y, Hisatsune T (2011) Cholinergic activation of hippocampal neural stem cells in aged dentate gyrus. *Hippocampus* **21**, 446-459.

[33] Jakubs K, Bonde S, Iosif RE, Ekdahl CT, Kokaia Z, Kokaia M, Lindvall O (2008) Inflammation regulates functional integration of neurons born in adult brain. *J Neurosci* **28**, 12477-12488.

[34] Verret L, Jankowsky JL, Xu GM, Borchelt DR, Rampon C (2007) Alzheimer's-type amyloidosis in transgenic mice impairs survival of newborn neurons derived from adult hippocampal neurogenesis. *J Neurosci* **27**, 6771-6780.

[35] Rodríguez JJ, Jones VC, Tabuchi M, Allan SM, Knight EM, LaFerla FM, Oddo S, Verkhratsky A (2008) Impaired adult neurogenesis in the dentate gyrus of a triple transgenic mouse model of Alzheimer's disease. *PLoS One* **3**, e2935.

[36] Demars M, Hu YS, Gadadhar A, Lazarov O (2010) Impaired neurogenesis is an early event in the etiology of familial Alzheimer's disease in transgenic mice. *J Neurosci Res* **88**, 2103-2117.

[37] Jin K, Galvan V, Xie L, Mao XO, Gorostiza OF, Bredesen DE, Greenberg DA (2004) Enhanced neurogenesis in Alzheimer's disease transgenic (PDGF-APPSw, Ind) mice. *Proc Natl Acad Sci U S A* **101**, 13363-13367.

[38] López-Toledano MA, Shelanski ML (2007) Increased neurogenesis in young transgenic mice overexpressing human APP(Sw, Ind). *J Alzheimers Dis* **12**, 229-240.

[39] Ermini FV, Grathwohl S, Radde R, Yamaguchi M, Staufenbiel M, Palmer TD, Jucker M (2008) Neurogenesis and alterations of neural stem cells in mouse models of cerebral amyloidosis. *Am J Pathol* **172**, 1520-1528.

[40] Yu Y, He J, Zhang Y, Luo H, Zhu S, Yang Y, Zhao T, Wu J, Huang Y, Kong J, Tan Q, Li XM (2009) Increased hippocampal neurogenesis in the progressive stage of Alzheimer's disease phenotype in an APP/PS1 double transgenic mouse model. *Hippocampus* **19**, 1247-1253.

[41] Sun B, Halabisky B, Zhou Y, Palop JJ, Yu G, Mucke L, Gan L (2009) Imbalance between GABAergic and glutamatergic transmission impairs adult neurogenesis in an animal model of Alzheimer's disease. *Cell Stem Cell* **5**, 624-633.

[42] Mu Y, Gage FH (2011) Adult hippocampal neurogenesis and its role in Alzheimer's disease. *Mol Neurodegener* **6**, 85.

[43] Richetin K, Leclerc C, Toni N, Gallopin T, Pech S, Roybon L, Rampon C (2015) Genetic manipulation of adult-born hippocampal neurons rescues memory in a mouse model of Alzheimer's disease. *Brain* **138**, 440-455.

[44] Kaneko N, Okano H, Sawamoto K (2006) Role of the cholinergic system in regulating survival of newborn neurons in the adult mouse dentate gyrus and olfactory bulb. *Genes Cells* **11**, 1145-1159.

[45] Jin K, Xie L, Mao XO, Greenberg DA (2006) Alzheimer's disease drugs promote neurogenesis. *Brain Res* **1085**, 183-188.

[46] Kotani S, Yamauchi T, Teramoto T, Ogura H (2008) Donepezil, an acetylcholinesterase inhibitor, enhances adult hippocampal neurogenesis. *Chem Biol Interact* **175**, 227-230.

[47] Islam MR, Moriguchi S, Tagashira H, Fukunaga K (2014) Rivastigmine improves hippocampal neurogenesis and depression-like behaviors via 5-HT1A receptor stimulation in olfactory bulbectomized mice. *Neuroscience* **272**, 116-130.

[48] Herculano B, Tamura M, Ohba A, Shimatani M, Kutsuna N, Hisatsune T (2013) β-alanyl-L-histidine rescues cognitive deficits caused by feeding a high fat diet in a transgenic mouse model of Alzheimer's disease. *J Alzheimers Dis* **33**, 983-997.

[49] Chin Y, Kishi M, Sekino M, Nakajo F, Abe Y, Terazono Y, Hiroyuki O, Kato F, Koizumi S, Gachet C, Hisatsune T (2013) Involvement of glial $P2Y_1$ receptors in cognitive

deficit after focal cerebral stroke in a rodent model. *J Neuroinflammation* **10**, 95.

[50] Lalonde R, Kim HD, Fukuchi K (2004) Exploratory activity, anxiety, and motor coordination in bigenic APPswe + PS1/DeltaE9 mice. *Neurosci Lett* **369**, 156-161.

[51] Reiserer RS, Harrison FE, Syverud DC, McDonald MP (2007) Impaired spatial learning in the APPSwe + PSEN1DeltaE9 bigenic mouse model of Alzheimer's disease. *Genes Brain Behav* **6**, 54-65.

[52] Cramer PE, Cirrito JR, Wesson DW, Lee CY, Karlo JC, Zinn AE, Casali BT, Restivo JL, Goebel WD, James MJ, Brunden KR, Wilson DA, Landreth GE (2012) ApoE-directed therapeutics rapidly clear β-amyloid and reverse deficits in AD mouse models. *Science* **335**, 1503-1506.

[53] Monje ML, Toda H, Palmer TD (2003) Inflammatory blockade restores adult hippocampal neurogenesis. *Science* **302**, 1760-1765.

[54] Ekdahl CT, Claasen JH, Bonde S, Kokaia Z, Lindvall O (2003) Inflammation is detrimental for neurogenesis in adult brain. *Proc Natl Acad Sci U S A* **100**, 13632-13637.

[55] Jakubs K, Nanobashvili A, Bonde S, Ekdahl CT, Kokaia Z, Kokaia M, Lindvall O (2006) Environment matters: Synaptic properties of neurons born in the epileptic adult brain develop to reduce excitability. *Neuron* **52**, 1047-1059.

[56] Jankowsky JL, Slunt HH, Ratovitski T, Jenkins NA, Copeland NG, Borchelt DR (2001) Co-expression of multiple transgenes in mouse CNS: A comparison of strategies. *Biomol Eng* **17**, 157-165.

[57] Jankowsky JL, Fadale DJ, Anderson J, Xu GM, Gonzales V, Jenkins NA, Copeland NG, Lee MK, Younkin LH, Wagner SL, Younkin SG, Borchelt DR (2004) Mutant presenilins specifically elevate the levels of the 42 residue beta-amyloid peptide *in vivo*: Evidence for augmentation of a 42-specific gamma secretase. *Hum Mol Genet* **13**, 159-170.

[58] Garcia-Alloza M, Robbins EM, Zhang-Nunes SX, Purcell SM, Betensky RA, Raju S, Prada C, Greenberg SM, Bacskai BJ, Frosch MP (2006) Characterization of amyloid deposition in the APPswe/PS1dE9 mouse model of Alzheimer disease. *Neurobiol Dis* **24**, 516-524.

[59] Volianskis A, Køstner R, Mølgaard M, Hass S, Jensen MS (2010) Episodic memory deficits are not related to altered glutamatergic synaptic transmission and plasticity in the CA1 hippocampus of the APPswe/PS1δE9-deleted transgenic mice model of ß-amyloidosis. *Neurobiol Aging* **31**, 1173-1187.

[60] Lalonde R, Kim HD, Maxwell JA, Fukuchi K (2005) Exploratory activity and spatial learning in 12-month-old APP(695)SWE/co+PS1/DeltaE9 mice with amyloid plaques. *Neurosci Lett* **390**, 87-92.

[61] Knafo S, Venero C, Merino-Serrais P, Fernaud-Espinosa I, Gonzalez-Soriano J, Ferrer I, Santpere G, DeFelipe J (2009) Morphological alterations to neurons of the amygdala and impaired fear conditioning in a transgenic mouse model of Alzheimer's disease. *J Pathol* **219**, 41-51.

[62] Santos MD, Alkondon M, Pereira EF, Aracava Y, Eisenberg HM, Maelicke A, Albuquerque EX (2002) The nicotinic allosteric potentiating ligand galantamine facilitates synaptic transmission in the mammalian central nervous system. *Mol Pharmacol* **61**, 1222-1234.

[63] Ohkawa N, Saitoh Y, Tokunaga E, Nihonmatsu I, Ozawa F, Murayama A, Shibata F, Kitamura T, Inokuchi K (2012) Spine formation pattern of adult-born neurons is differentially modulated by the induction timing and location of hippocampal plasticity. *PLoS One* **7**, e45270.

[64] Kee N, Teixeira CM, Wang AH, Frankland PW (2007) Imaging activation of adult-generated granule cells in spatial memory. *Nat Protoc* **2**, 3033-3044.

[65] Cao D, Lu H, Lewis TL, Li L (2007) Intake of sucrose-sweetened water induces insulin resistance and exacerbates memory deficits and amyloidosis in a transgenic mouse model of Alzheimer disease. *J Biol Chem* **282**, 36275-36282.

[66] Corcoran KA, Lu Y, Turner RS, Maren S (2002) Overexpression of hAPPswe impairs rewarded alternation and contextual fear conditioning in a transgenic mouse model of Alzheimer's disease. *Learn Mem* **9**, 243-252.

[67] Ikonomovic MD, Abrahamson EE, Isanski BA, Debnath ML, Mathis CA, Dekosky ST, Klunk WE (2006) X-34 labeling of abnormal protein aggregates during the progression of Alzheimer's disease. *Methods Enzymol* **412**, 123-144.

[68] Hering H, Sheng M (2001) Dendritic spines: Structure, dynamics and regulation. *Nat Rev Neurosci* **2**, 880-888.

[69] von Bohlen Und Halbach O (2009) Structure and function of dendritic spines within the hippocampus. *Ann Anat* **191**, 518-531.

[70] Gao X, Arlotta P, Macklis JD, Chen J (2007) Conditional knock-out of beta-catenin in postnatal-born dentate gyrus granule neurons results in dendritic malformation. *J Neurosci* **27**, 14317-14325.

[71] Revest JM, Dupret D, Koehl M, Funk-Reiter C, Grosjean N, Piazza PV, Abrous DN (2009) Adult hippocampal neurogenesis is involved in anxiety-related behaviors. *Mol Psychiatry* **14**, 959-967.

[72] Town T, Nikolic V, Tan J (2005) The microglial "activation" continuum: From innate to adaptive responses. *J Neuroinflammation* **2**, 24.

[73] Hanisch UK, Kettenmann H (2007) Microglia: Active sensor and versatile effector cells in the normal and pathologic brain. *Nat Neurosci* **10**, 1387-1394.

[74] Greig NH, Utsuki T, Ingram DK, Wang Y, Pepeu G, Scali C, Yu QS, Mamczarz J, Holloway HW, Giordano T, Chen D, Furukawa K, Sambamurti K, Brossi A, Lahiri DK (2005) Selective butyrylcholinesterase inhibition elevates brain acetylcholine, augments learning and lowers Alzheimer beta-amyloid peptide in rodent. *Proc Natl Acad Sci U S A* **102**, 17213-17218.

[75] Naik RS, Hartmann J, Kiewert C, Duysen EG, Lockridge O, Klein J (2009) Effects of rivastigmine and donepezil on brain acetylcholine levels in acetylcholinesterase-deficient mice. *J Pharm Pharm Sci* **12**, 79-85.

[76] Penzes P, Cahill ME, Jones KA, VanLeeuwen JE, Woolfrey KM (2011) Dendritic spine pathology in neuropsychiatric disorders. *Nat Neurosci* **14**, 285-293.

[77] Games D, Adams D, Alessandrini R, Barbour R, Berthelette P, Blackwell C, Carr T, Clemens J, Donaldson T, Gillespie F (1995) Alzheimer-type neuropathology in transgenic mice overexpressing V717F beta-amyloid precursor protein. *Nature* **373**, 523-527.

[78] Mucke L, Masliah E, Yu GQ, Mallory M, Rockenstein EM, Tatsuno G, Hu K, Kholodenko D, Johnson-Wood K, McConlogue L (2000) High-level neuronal expression of abeta 1-42 in wild-type human amyloid protein precursor transgenic mice: Synaptotoxicity without plaque formation. *J Neurosci* **20**, 4050-4058.

[79] Lanz TA, Carter DB, Merchant KM (2003) Dendritic spine loss in the hippocampus of young PDAPP and Tg2576 mice and its prevention by the ApoE2 genotype. *Neurobiol Dis* **13**, 246-253.

[80] Pozueta J, Lefort R, Shelanski ML (2013) Synaptic changes in Alzheimer's disease and its models. *Neuroscience* **251**, 51-65.

[81] Erion JR, Wosiski-Kuhn M, Dey A, Hao S, Davis CL, Pollock NK, Stranahan AM (2014) Obesity elicits interleukin 1-mediated deficits in hippocampal synaptic plasticity. *J Neurosci* **34**, 2618-2631.

[82] Yang G, Parkhurst CN, Hayes S, Gan WB (2013) Peripheral elevation of TNF-α leads to early synaptic abnormalities in the mouse somatosensory cortex in experimental autoimmune encephalomyelitis. *Proc Natl Acad Sci U S A* **110**, 10306-10311.

[83] Zou C, Shi Y, Ohli J, Schüller U, Dorostkar MM, Herms J (2016) Neuroinflammation impairs adaptive structural plasticity of dendritic spines in a preclinical model of Alzheimer's disease. *Acta Neuropathol* **131**, 235-246.

[84] Pollak Y, Gilboa A, Ben-Menachem O, Ben-Hur T, Soreq H, Yirmiya R (2005) Acetylcholinesterase inhibitors reduce brain and blood interleukin-1beta production. *Ann Neurol* **57**, 741-745.

[85] Yirmiya R, Goshen I (2011) Immune modulation of learning, memory, neural plasticity and neurogenesis. *Brain Behav Immun* **25**, 181-213.

[86] Kosasa T, Kuriya Y, Matsui K, Yamanishi Y (1999) Effect of donepezil hydrochloride (E2020) on basal concentration of extracellular acetylcholine in the hippocampus of rats. *Eur J Pharmacol* **380**, 101-107.

[87] Trabace L, Coluccia A, Gaetani S, Tattoli M, Cagiano R, Pietra C, Kendrick KM, Cuomo V (2000) *In vivo* neurochemical effects of the acetylcholinesterase inhibitor ENA713 in rat hippocampus. *Brain Res* **865**, 268-271.

[88] Scali C, Casamenti F, Bellucci A, Costagli C, Schmidt B, Pepeu G (2002) Effect of subchronic administration of metrifonate, rivastigmine and donepezil on brain acetylcholine in aged F344 rats. *J Neural Transm (Vienna)* **109**, 1067-1080.

[89] Amenta F, Tayebati SK, Vitali D, Di Tullio MA (2006) Association with the cholinergic precursor choline alphoscerate and the cholinesterase inhibitor rivastigmine: An approach for enhancing cholinergic neurotransmission. *Mech Ageing Dev* **127**, 173-179.

[90] Liang YQ, Tang XC (2006) Comparative studies of huperzine A, donepezil, and rivastigmine on brain acetylcholine, dopamine, norepinephrine, and 5-hydroxytryptamine levels in freely-moving rats. *Acta Pharmacol Sin* **27**, 1127-1136.

[91] Shytle RD, Mori T, Townsend K, Vendrame M, Sun N, Zeng J, Ehrhart J, Silver AA, Sanberg PR, Tan J (2004) Cholinergic modulation of microglial activation by alpha 7 nicotinic receptors. *J Neurochem* **89**, 337-343.

[92] De Simone R, Ajmone-Cat MA, Carnevale D, Minghetti L (2005) Activation of alpha7 nicotinic acetylcholine receptor by nicotine selectively up-regulates cyclooxygenase-2 and prostaglandin E2 in rat microglial cultures. *J Neuroinflammation* **2**, 4.

[93] Wang ZF, Tang XC (2007) Huperzine A protects C6 rat glioma cells against oxygen-glucose deprivation-induced injury. *FEBS Lett* **581**, 596-602.

[94] Matsumura A, Suzuki S, Iwahara N, Hisahara S, Kawamata J, Suzuki H, Yamauchi A, Takata K, Kitamura Y, Shimohama S (2015) Temporal changes of CD68 and α7 nicotinic acetylcholine receptor expression in microglia in Alzheimer's disease-like mouse models. *J Alzheimers Dis* **44**, 409-423.

[95] Wang H, Liao H, Ochani M, Justiniani M, Lin X, Yang L, Al-Abed Y, Metz C, Miller EJ, Tracey KJ, Ulloa L (2004) Cholinergic agonists inhibit HMGB1 release and improve survival in experimental sepsis. *Nat Med* **10**, 1216-1221.

Supplementary Table 1. Composition of feed used in this study

Composition	MF	HFD-32
Water (g/100 g)	7.9	6.2
Protein (g/100 g)	23.1	25.5
Fat (g/100 g)	5.1	32
Fiber (g/100 g)	2.8	2.9
Ash (g/100 g)	5.8	4.0
Nitrogen-free extract (g/100 g)	55.3	29.4
Calories (kcal/100 g)	359	508
Calories from fat (%)	12.8	56.7

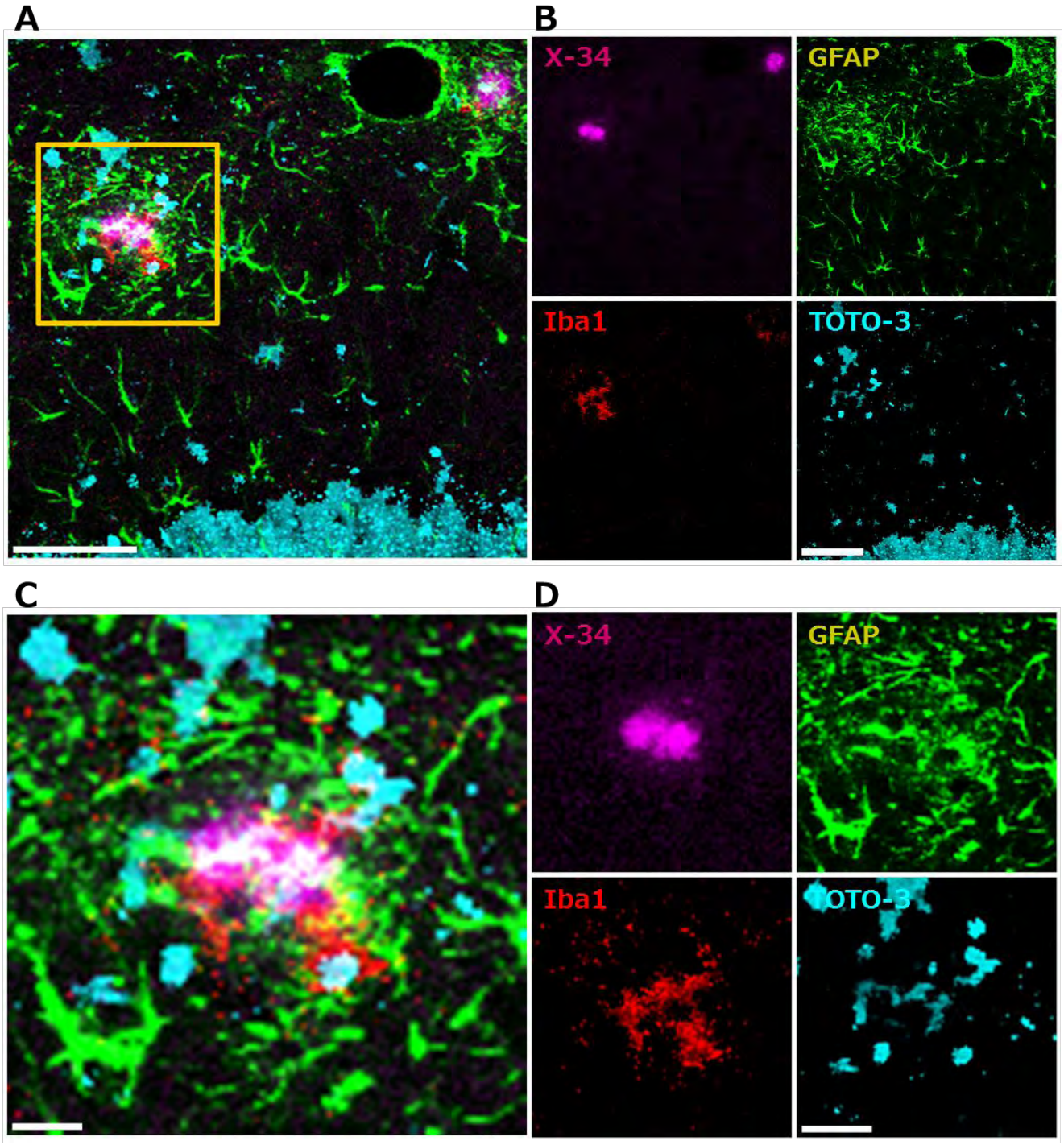

Supplementary Figure 1. Senile plaques are surrounded by cell aggregates composed of reactive astrocytes and microglia.

Quadruple labeling of hippocampal sections for X-34 (Magenta), GFAP (green), Iba1 (red), and TOTO-3 (cyan). We labeled senile plaques in the hippocampus with X-34 after the GFAP/Iba1/TOTO-3 labeling described in the Methods section. **(A)** Representative image of this quadruple labeling in the hippocampus of Tg mice. Scale bar, 50 μm. **(B)** Single-channel images of the overlay micrograph. Scale bar, 50 μm. **(C)** Magnified view of the yellow-boxed area. This panel shows the composite image of a representative immunostained senile plaque in the Tg mice. Scale bar, 5 μm. **(D)** Four panels showing each single-channel micrograph. Scale bar, 10 μm. The X-34-labeled senile plaque was surrounded by activated astrocytes and microglia.

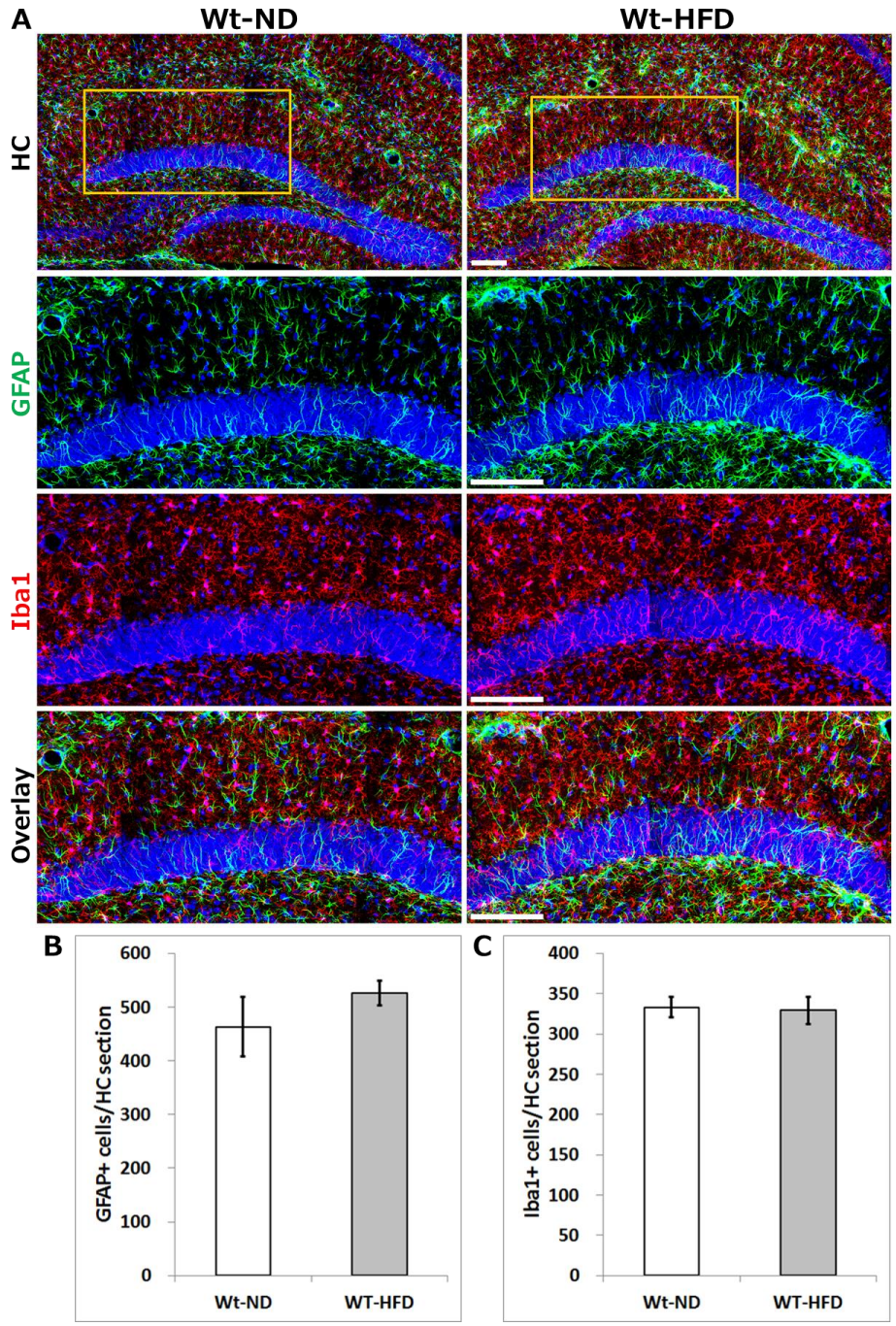

Supplementary Figure 2. HFD alone does not significantly affect inflammation in the hippocampus of Wt mice.

In this pilot study, ND-maintained 4-month-old Wt mice were treated with ND or HFD for the next 8 weeks. The 6-month-old Wt-ND mice and Wt-HFD mice were then transcardially perfused and their brain was fixed as described in the Methods section. The hippocampal sections were labeled and analyzed for GFAP+ and Iba1+ cells as described in the Methods section. **(A)** Representative images of hippocampal sections triple labeled for GFAP (green), Iba1 (red), and DAPI (blue). Lower panels show magnified views. The GFAP-labeled astrocytes and Iba1-labeled microglia in the Wt-HFD mice were relatively quiescent in the hippocampus, similar to the Wt-ND mice. There were no microaggregates of activated astrocytes and microglia in the Wt-HFD mice. Scale bar, 50 µm (upper panel); 10 µm (lower panels). **(B)** Average number of GFAP-immunopositive cells per coronal section in the hippocampus. **(C)** Average number of Iba1-immunopositive cells per coronal section in the hippocampus. The number of GFAP+ astrocytes and Iba1+ microglia was similar in the Wt-ND and Wt-HFD mice ($p > 0.05$, not significant, two-tailed Student's t-test). Data represent the mean ± SEM; n = 3 per group. HC, hippocampus; Wt, wild-type; ND, normal diet; HFD, high-fat diet.